Observation of the circulation in the Newfoundland Basin in winter 1997

G Caniaux, L Prieur, H Giordani, F Hernandez, L Eymard

Observation of the Circulation in the Newfoundland Basin in Winter 1997

G. CANIAUX

Centre National de Recherches Météorologiques, Toulouse, France

L. PRIEUR

Laboratoire de Physique et Chimie Marines, Villefranche-sur-mer, France

H. GIORDANI

Centre National de Recherches Météorologiques, Toulouse, France

F. HERNANDEZ

CLS Argos, Ramonville Saint-Agne, France

L. EYMARD

Centre d'Études Terrestres et Planétaires, Velizy, France

(Manuscript received 15 July 1999, in final form 12 May 2000)

ABSTRACT

A hydrographic survey was performed in January–February 1997 to document the winter circulation of the North Atlantic Current system in the Newfoundland Basin, as part of the Fronts and Atlantic Storm Tracks Experiment (FASTEX). Eighty-seven conductivity–temperature–depth (CTD) stations were occupied along a four-section trapezoid, which spanned the ''Northwest Corner'' and the branching of the North Atlantic Current along 35°W. Realistic sea surface temperature analyses were produced every 15 days, using all available data collected in this area during the two months of the FASTEX experiment. These maps were combined with sea level anomaly fields from the TOPEX/Poseidon and *ERS-2* satellites at the same time intervals to analyze the features of the main currents in the area and their evolution. These combined analyses, providing a coherent overview of the fronts and jets identified along the ship track, and the CTD stations are further used to estimate their transports. The general pattern is a 15 Sv (Sv $\equiv 10^6$ m^3 s^{-1}) transport by the North Atlantic Current at 47°N, 43°W, the existence of a recirculating gyre inside the Northwest Corner, and a complex branching of the circulation associated with significant surface fronts. The recirculating gyre forms a closed circulation, in which a very deep warm eddy, 100 km wide, was sampled at the end of February: its mixed layer was 800 m deep and its transport was 27 Sv. Along 35°W, three fronts were identified between 45° and 52°N: the Northern Subarctic Front, the Southern Subarctic Front, and the Mid-Atlantic Front, whose origins are precisely located. The currents associated with these fronts transport 26 Sv toward the east before crossing the Mid-Atlantic Ridge and supplying the eastern part of the North Atlantic basin. An important transport (14 Sv) was calculated near 46°N, 37°W, which mostly fed the current associated with the Mid-Atlantic Front.

1. Introduction

The oceanic circulation off Newfoundland is complex and has captured the attention of oceanographers for a relatively long time. The most significant feature of the area is the North Atlantic Current (NAC), which transports large quantities of warm and saline subtropical water to the northeast. It is unique among other western boundary currents in transporting such waters so high in latitude (Rossby 1996) and it plays an important role in temperating the climate of Western Europe in winter (Krauss 1986).

The NAC is the northern branch issued from the Gulf Stream after its passage over the Newfoundland Rise (Lozier et al. 1995; Kearns and Rossby 1998; Rossby 1999). Its northward trajectory follows the continental slope and is strongly locked to the bathymetry until 51°N (Rossby 1996) (Fig. 1). Along the Newfoundland plateau, the NAC is in contact with the cold and fresh

Corresponding author address: Dr. G. Caniaux, CNRM, 42, Av. G. Coriolis, 31057 Toulouse Cedex, France.
E-mail: caniaux@meteo.fr

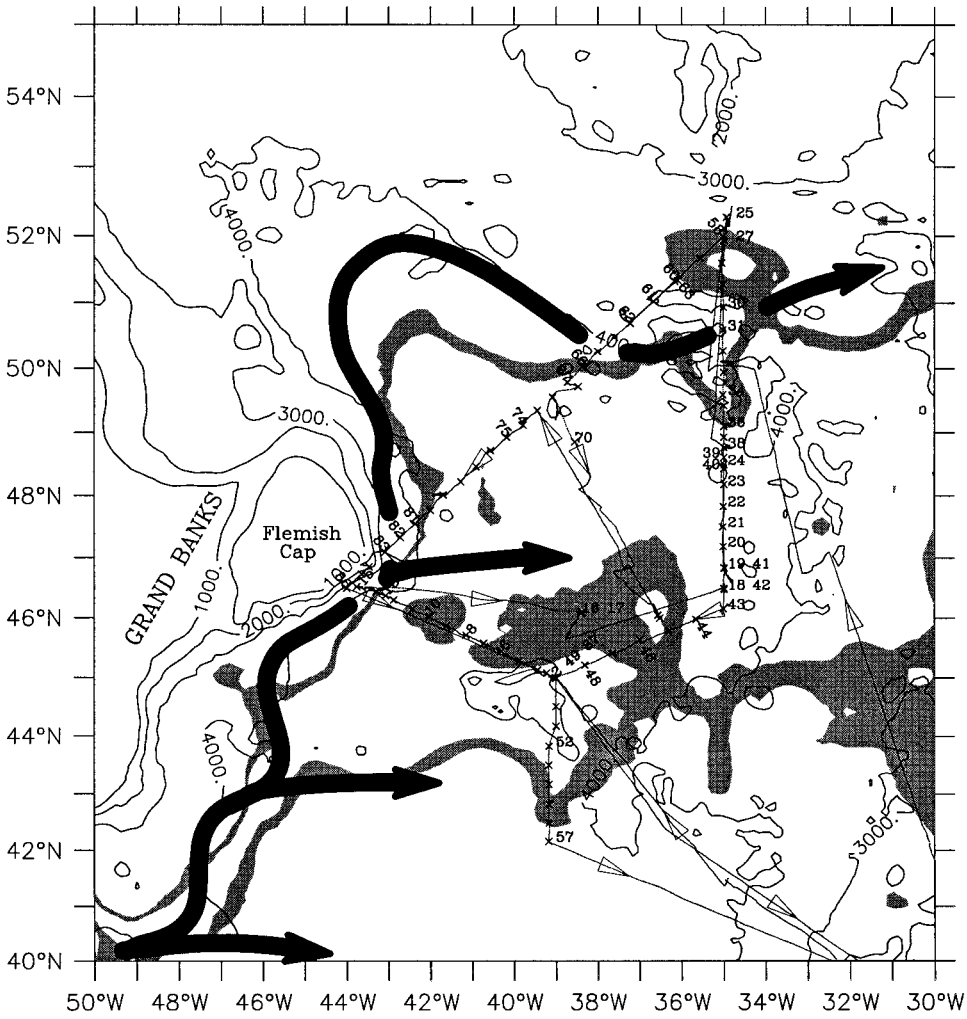

FIG. 1. Ship track of R/V *Le Suroît* during the two legs: the open arrows indicate the direction along the track and crosses the CTD stations with corresponding number. The 1000, 2000, 3000, and 4000-m isobaths are indicated. A schematic of the North Atlantic Current system (black arrows) is represented from Rossby (1996) and Kearns and Rossby (1999, submitted to *J. Geophys. Res.*). Superimposed in gray, SST bands correspond to the position of the main fronts found in this study and redrawn from Fig. 9c. These bands delimit 10°–11°C in the northern part of the figure (pathway of the NAC) and 14°–15°C in the southern part (see text). Note the rather good correspondence of the climatological position of the NAC and its position in this study.

Labrador Sea Water (Reynaud et al. 1995), and the convergence of these two contrasting waters reinforces the density gradients, providing a considerable source of energy for the NAC (Krauss et al. 1990). Towards 51°N, the NAC turns eastward in a permanent structure called ''the NorthWest Corner'' (NWC hereafter: Worthington 1976; Lazier 1994), and then flows eastward, broader, and more diffuse toward the Mid-Atlantic Ridge.

In the Newfoundland basin, the NAC circulation is mainly dominated by eddies, meanders, and recirculation gyres (Mann 1967; Schmitz and McCartney 1993) and satellite-tracked drifting buoys (Käse and Krauss 1996) and altimetry confirm a high mesoscale variability and sharp gradients of eddy kinetic energy in this region (Richardson 1983; Le Traon et al. 1990; Brügge 1995). The circulation is also complex because the NAC splits into several branches with their associated fronts (Dietrich et al. 1980). These fronts and their water masses are difficult to identify in this region due to their large temporal and spatial variability (Fofonoff and Hendry 1985; Arhan et al. 1989; Belkin and Levitus 1996), and consequently transport calculations are highly variable. According to Schmitz and McCartney (1993), uncertainties in transport estimates may be as high as 25% in this region.

Climatological studies in this basin (Kearns and Rossby 1998, 1999, submitted to *J. Geophys. Res.*) indicate that, despite some regional differences, the circulation pattern does not vary much from one season to another, suggesting that variability remains high throughout the

year. However, offshore data coverage is poor in some seasons (mainly fall and winter), which limits the accurate quantification of the seasonal NAC variability.

In spite of the numerous studies devoted to the Newfoundland Basin, the wintertime circulation is poorly known. Few systematic hydrographic surveys have been carried out and measurements are restricted to floats (Rossby 1996; Carr et al. 1997), drifting buoys (Krauss 1986; Brügge 1995) or current meter moorings (Colin de Verdière et al. 1989; Lazier 1994).

In this study we first present the results of the only (to our knowledge) midwinter survey performed in this area (section 2). The survey was made in January–February 1997 during the Couplage avec l'Atmosphère en Conditions Hivernales (CATCH) experiment (Eymard et al. 1999), part of the Fronts and Atlantic Storm Tracks Experiment (FASTEX, Joly et al. 1999).

Second, we propose a new methodology to study and monitor the wintertime circulation in this area with only the help of surface parameters. Sea surface temperature analyses (section 3) were produced from volunteer observation ships and surface drifters and current fields (section 4) were derived from altimetric data. Both analyses were validated with data collected during the hydrographic survey. Furthermore, these analyses put the hydrographic results into a broader context by presenting the space and time evolution of the surface temperatures and currents. Finally the surface currents and hydrographic data are combined to provide a consistent pattern of the circulation (section 5). A representation of the main fronts found in this study (redrawn from Fig. 9) has been superimposed on Fig. 1 (with the historical climatological pattern) to afford the reader a view of the overall circulation reconstructed in the next sections.

2. Hydrography

In this section the hydrographic survey performed during the CATCH experiment is analyzed to identify the different fronts, water masses, and currents observed during the cruise; the characteristics of distinct water masses and the depths at which fronts could be identified, their nature, and their denomination from previous studies will thus be precise.

The ship R/V *Le Suroît* was equipped with a SEABIRD SBE21 SEACAT thermosalinograph and a 150-kHz acoustic Doppler current profiler (ADCP), which enabled continuous measurements of sea surface temperature SST, sea surface salinity (SSS), and currents (0–150 m). During the two months of the experiment, 87 conductivity–temperature–depth (CTD SEABIRD SBE9) casts were collected. This survey consisted of four sections (Table 1) with CTD profiles between the surface and 2000 m, every 10–20 nautical miles. The sections constitute a trapezoidal survey (Fig. 1) designed to span the Labrador Current in the northwest, the NWC along the northern section, and the different branches of the NAC in the eastern section.

TABLE 1. Characteristics of the sections of the hydrographic survey: dates, lengths, number of CTD performed, and station number.

Section	Date	Length (km)	Number of CTD	Station number
West	13–17 Jan	400	13	2–15
East	21–28 Jan	680	23	18–43
South	29 Jan	300	6	43–49
South2	30–31 Jan	300	8	49–57
North	11–25 Feb	900	24	58–86

The survey was split into two legs. The first from 8 January to 3 February covered the western, eastern, and southern sections with an extension toward 42°N (called section south2 hereafter). After a short stop in Horta (Azores), the second leg from 4 February to 3 March continued along the longest, northern section and was interrupted for 6 days (15 to 21 February) due to the operational constraints of the FASTEX experiment. The point located 45°N, 39°W was visited three times (on 12 and 29 January and on 27 February) as a fixed reference point.

In Fig. 2, each section is presented as potential temperature and salinity versus density profiles and as a density versus depth profile in order to identify possible property fronts and their relationship to the dynamical fronts. The dynamical fronts were determined from the density at 300 m, the depth at which the main currents are expected to be strongest (Arhan 1990). The property fronts can be identified from sharp temperature and salinity characteristics but a smooth density gradient in the mixed layer. The location of fronts is indicated with asterisks in Fig. 2. In Fig. 2, the sections have been arranged such that the beginning (or end) of one section faces the end (or beginning) of the contiguous section and they will be discussed in this order (south2, south, east, west, and north), despite their chronology. Along-track ADCP currents are plotted in Figs. 3a,b. These data were collected at 6-min intervals but, for clarity, were subsampled and plotted every 10 km. The fronts identified along the ship trajectory from the CTD sections, or suggested from the thermosalinograph data, are positioned in Figs. 3a,b. An overview of the different water masses collected is presented as a θ–S diagram in Fig. 4. Five distinct water masses were identified according to the classification of Krauss et al. (1990) and Arhan (1990):

- North Atlantic Central Water (NACW: 7°C $\leq \theta \leq$ 17°C and $S \geq 35$ psu) generally with a tight θ–S relationship, overlaying, at $\sigma_\theta \geq 27.3$ the
- SubArctic Intermediate Water (SAIW: 4°C $\leq \theta \leq$ 9°C and $S \leq 35.1$ psu) with sometimes an influence of
- Mediterranean Water (MW: 4°C $\leq \theta \leq$ 9°C and $S \leq$ 35.1 psu),
- Labrador Current Water (LCW: $\theta \leq$ 4°C and $S \leq 34.8$ psu), and

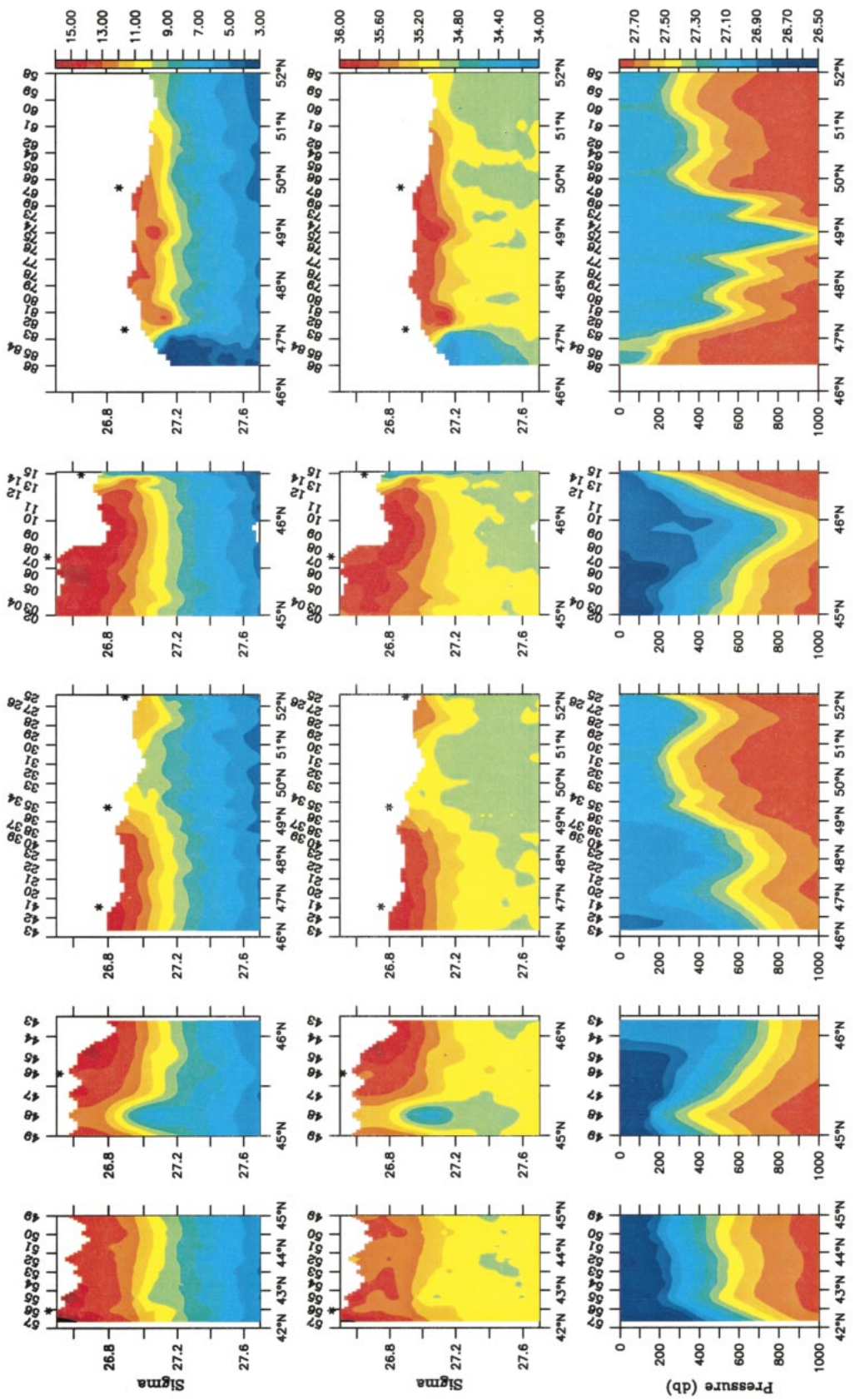

FIG. 2. Potential temperature (top row in °C), salinity (middle), potential density anomaly (bottom in kg m^{-3}) cross section along: the two southern (first two columns), eastern (third column), western (fourth column), and northern (fifth column) sections. Stars indicate the position of the main fronts. The station numbers are indicated above each plot.

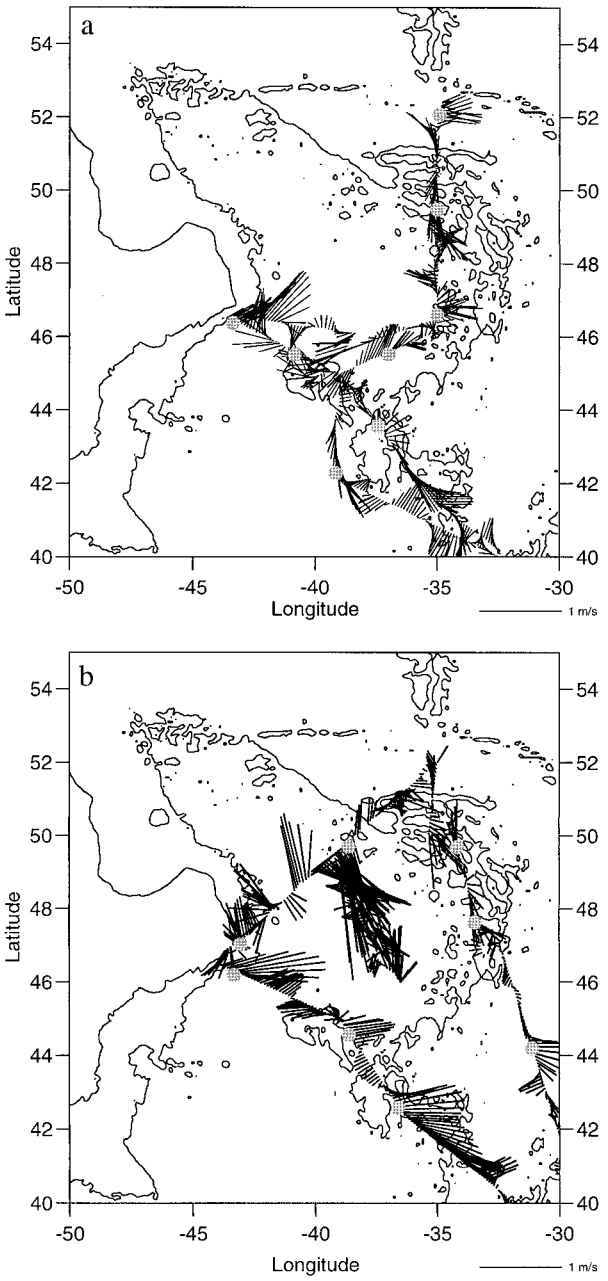

FIG. 3. ADCP currents along the ship track (a) leg 1, from 8 Jan to 3 Feb and (b) leg 2, from 4 Feb to 1 Mar. Currents were plotted every 10 km. The 2000- and 4000-m isobaths are superimposed. Large dots indicate the position of the main fronts identified along the survey.

- North Atlantic Deep Water (NADW: $\theta \leq 4$°C and $34.8 \leq S \leq 35$ psu).

Some CTD profiles were selected (Fig. 5) as representative of the water mass collected along each section because the water masses identified during the experiment were not sampled along the same sections.

a. Section south2 (stations 49–57)

Along section south2 density is quite homogeneous at 300 m (Fig. 2, first column) except in the south near 42°N (station 57), where we enter into the least dense water of all our samples. Here, the surface waters and those at 300-m depth had temperature higher than 16°C and salinity higher than 36 psu. A strong density gradient was also observed across the entire thermocline down to 1000 m. This front was associated with a southeastward current observed before reaching the warm side of the front (Fig. 3a), meaning that it was meandering and oriented northwest–southeast. NACW was found along the whole section across the main thermocline. At station 57 an influence of MW is suggested between 800 and 1200 m (Fig. 5d). We infer that this front may be the so-called Mediterranean Water Front (MWF), which has the same properties as described by Belkin and Levitus (1996), and coincides with the northwestern extension of a MW tongue at intermediate depths, with a pronounced influence in the layer 800–1200 m (Sy et al. 1992; Arhan and King 1995). Belkin and Levitus found this front at 39°N, 35°W: 3° farther southeast from our location. However, that no other front or lower density surface water were detected with the thermosalinograph between the Azores and station 57 strongly suggests that we crossed the MWF at this higher latitude.

b. The southern section (stations 43–49)

A strong northeastward current was detected between 45.5°N, 37°W and 45°N, 38°W (Fig. 3a). Less dense water was sampled east of this jet, with a sharp density gradient at 300 m between station 46 and 47 (Fig. 2), meaning that a dynamical front was crossed at this location. NACW was found along the entire section, except for station 48 where a sharply cyclonic feature shoals near 200 m with SAIW (Fig. 2, column 2 and Fig. 5d). The presence of MW was also detected at depths of 800–1000 m in some profiles (station 46, Fig. 5d). Because the same water properties were collected during the eastern section, this front will be referred as the Mid-Atlantic Front (MAF), separating $\sigma_{300} = 26.9$ ($T_{300} = 13°–14°$C and $S_{300} = 35.6–35.8$ psu) waters on its warm side from $\sigma_{300} = 27.0$ ($T_{300} = 10°–12°$C and $S_{300} = 35.2–35.6$ psu) waters on its cold side. Note the presence of a shallow (less than 300 m deep) discontinuity between stations 44 and 45 (Fig. 2, column 2): at this spot, isopycnals outcrop at the surface and the density gradient reverses below 300 m.

c. The eastern section (stations 18–43)

This section runs along 35°W, a transect already investigated by Russian ships during the period 1976–85 (Belkin and Levitus 1996) and during the French–German experiment program TOPOGULF (Sy 1988; Har-

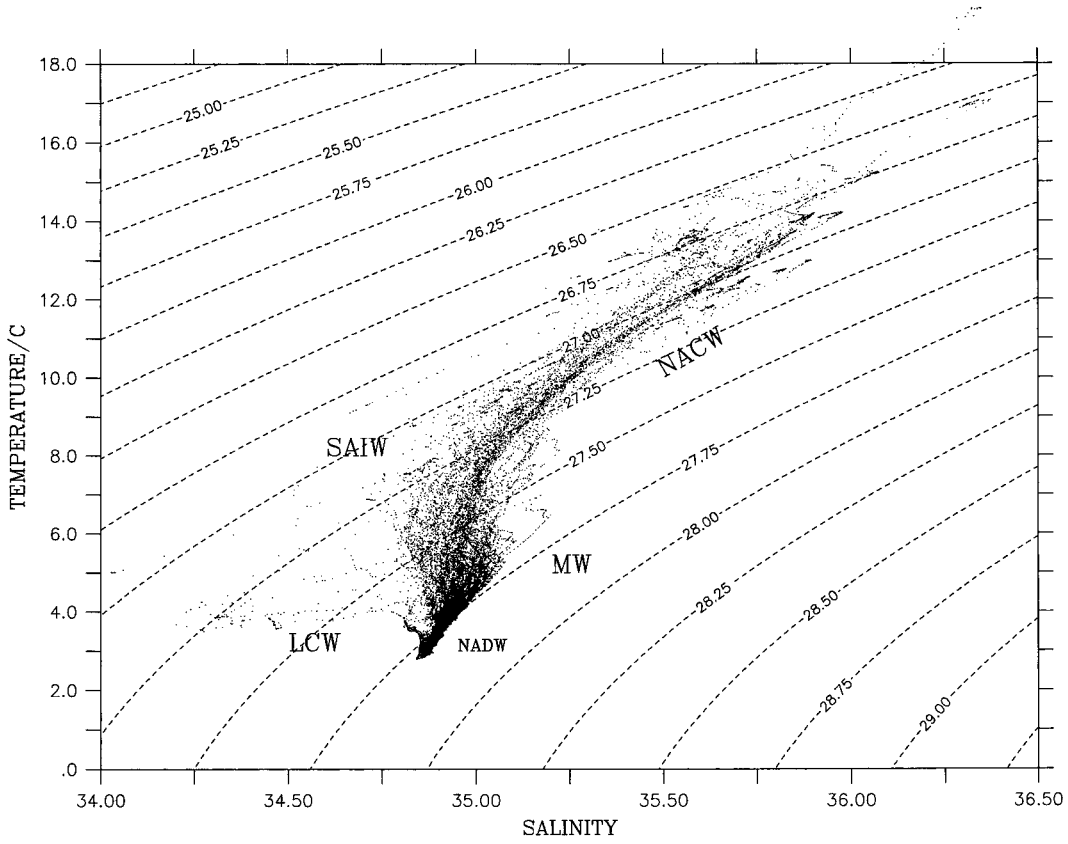

FIG. 4. Diagram of salinity vs potential temperature from all the hydrographic stations shown in Fig. 1. North Atlantic Central Water (NACW), Mediterranean Water (MW), North Atlantic Deep Water (NADW), SubArctic Intermediate Water (SAIW), and Labrador Current Water (LCW) classes were adapted from Krauss et al. (1990) and Arhan (1990).

vey and Arhan 1988; Arhan 1990). The section was sampled in both directions (northward and southward) and cut through the branches of the NAC system. Three fronts were identified in reference with the aforementioned studies (Fig. 2, column 3):

- The southernmost front near 47°N separates σ_{300} = 26.9 waters from σ_{300} = 27.1, with a weak surface signature. An eastward flow (60 cm s^{-1}) was associated with this front (Fig. 3a). The warmer and saltier waters south of 47°N are essentially ''pure'' NACW (station 43, Fig. 5b), according to the classification of Harvey and Arhan (1988). This front had the same signature as the Mid-Atlantic Front (MAF) identified by Belkin and Levitus (1996) but with higher density values in surface. This front marks the northern limit of the pure NACW.
- A second front was observed at 49.5°N between stations 35 and 36, with clear 300 m and surface signature, separating σ_{300} = 27.1 (T_{300} = 12°C and S_{300} = 35.6 psu) waters on its warm side from σ_{300} = 27.3 (T_{300} = 6°C and S_{300} = 34.8 psu) waters on its cold side. This front was associated with a southeastward current that was found veering southward some distance farther north (Fig. 3a), indicating the presence of a meander. South of 49.5°N, NACW is characteristic and underlaid by SAIW (station 40, Fig. 5b). A rather loose θ–S relationship exists between 49.5°N and 52°N (stations 27–38: see station 36, Fig. 5b) and displaced to the left of the previous NACW profiles: this indicates the presence of the intermediate water or ''modified NACW'' (Harvey and Arhan 1986). Consequently this front corresponds to the South SubArctic Front (SSAF) of Belkin and Levitus (1996), which is one of the most permanent features of the region.
- Colder surface waters (7°–8°C) were found north of 52°N, with outcropping SAIW at station 25 (Fig. 5b). This front associated with an eastward current (Fig. 3a) is identified as the North SubArctic Front (NSAF) of Belkin and Levitus (1996). It delimits the extension of pure SAIW to the south (Arhan 1990). Shoaling of isopycnals between 50° and 51°N (Fig. 2, column 3) and farther north, the presence of less dense waters between 51° and 52°N indicated meanders along the NSAF. Modified NACW were identified at stations 30, 31, and 34 meaning strong SAIW and NACW mixing.

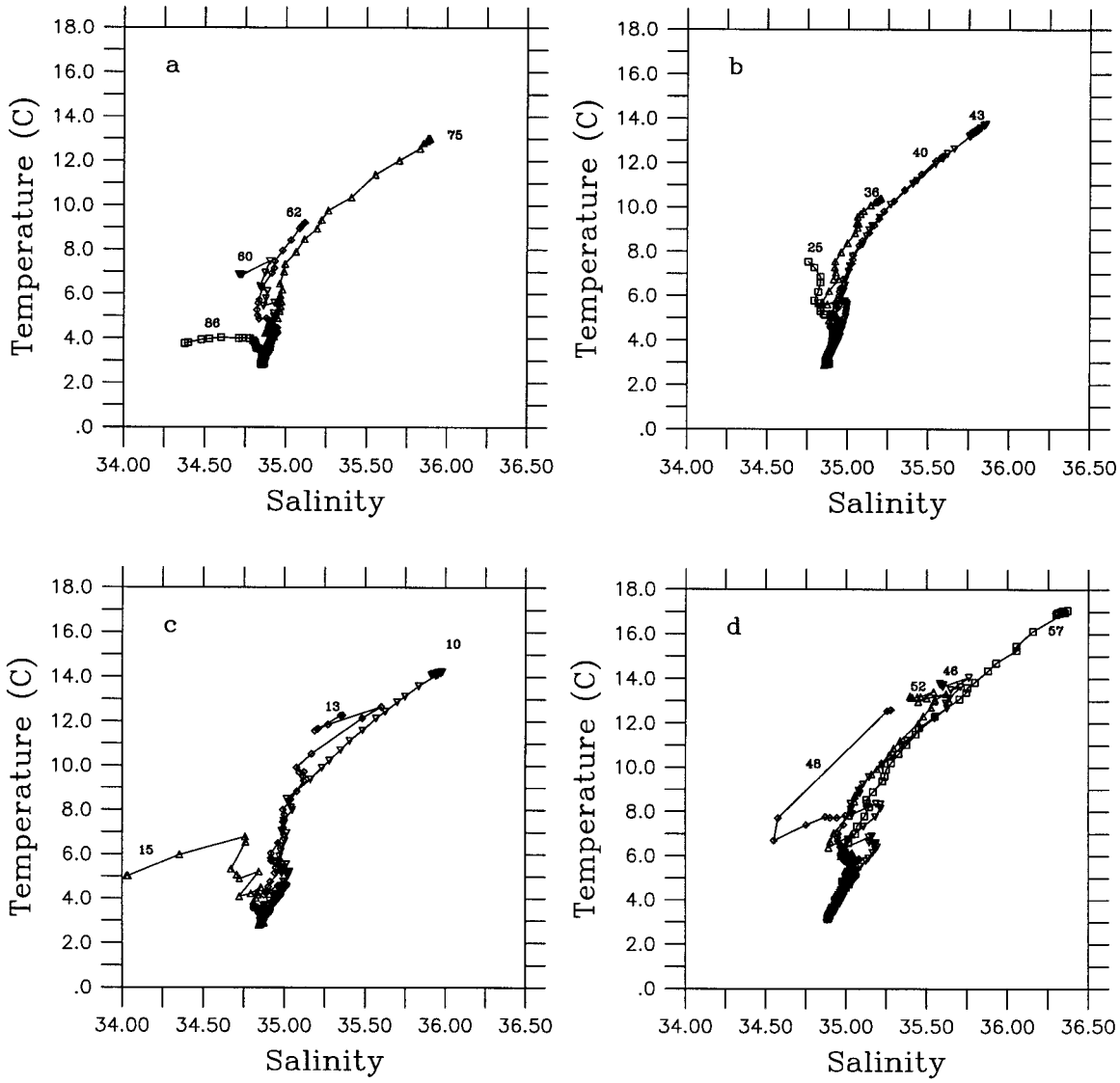

FIG. 5. Diagram of salinity vs potential temperature of some characteristic stations along: (a) the northern, (b) eastern, (c) western, and (d) southern sections. The stations are located in Fig. 1.

d. The western section (stations 2–15)

This section (Fig. 2, column 4) was run from the southeast to the northwest at the beginning of the experiment. A front associated with a westward current was crossed near station 7 at 45.5°N, 41°W (Fig. 3a). This front separated weakly contrasting surface waters (14° to 15°C), but a clearly defined density gradient exists at 300 m depth, with densities less than 26.9 on the northern side and greater than 27 on the southern side (Fig. 2, column 4). Note the reverse of density gradient between 300 m and the surface.

The NAC was found between stations 12 and 15, just southeast of the Grand Banks (Flemish Cap). Surface temperatures dropped from 13° to 5°C and salinity from 35.7 to 34.2 psu within 70 km. ADCP measurements registered a northeastward current with a maximum speed of more than 70 cm s^{-1} (Fig. 3a). Note the anticyclonic curvature of the flow just offshore of the NAC with deep mixed layers of 400–500 m (Fig. 2, column 4 and Fig. 3a). NACW was found all along the section except at station 15 where SAIW was identified up to the surface and at stations 13 and 14 where LCW and NACW were mixed in the upper 1000 m (station 13, Fig. 5c).

The western section was rerun from northwest to southeast at the end of the experiment (Fig. 1). The thermosalinograph measurements observed the same features as in January. However, the weak surface front was spatially shifted southeastward at 45°N, 39°W with a reverse of the flow (Fig. 3b) and a cooling was ob-

served when compared with the January measurements: nearly 0.7° to 1°C due to strong heat loss throughout the experiment (Eymard et al. 1999).

e. The northern section (stations 58–86)

This section (Fig. 2, column 5) can be divided into three parts:

- The northeastern segment (stations 58 to 66) where the water masses exhibit the same characteristics as the northern end of the eastern section with mixed NACW and SAIW. SAIW outcropped at station 60 (Fig. 5a) and 66. Again we infer that this part of the survey crossed the mixing zone between the NSAF and the SSAF. However, the surface waters were more dense, compared with the same waters collected along the eastern section, due to atmospheric forcing (increased evaporation and surface cooling).
- The middle segment (stations 67 to 82) is located inside the NWC, with less dense water and NACW in the upper 1000 m of the water column (station 75, Fig. 5a). The two fronts delimiting this segment were crossed at 50°N, 38.5°W (SST change from 12° to 7°C and SSS from 35.6 to 34.8 psu) and at 47°N, 43°W (SST change from 12° to 4°C and SSS from 35.6 to 34.2 psu) (Fig. 2, column 5). Along this segment, the current is dominated by strong inflow–outflow pairs reaching locally up to 80 cm s^{-1}, indicating the presence of eddies or meanders nearly 100 km wide (Fig. 3b). Note the exceptional mixed layer depth (800 m) registered at station 75 (Fig. 2, bottom of column 5).
- The last segment (stations 83 to 86) crossed the cold side of the NAC (Fig. 2, column 5). SAIW was in contact with the surface and temperature dropped to 3.8°C and salinity to 34.2 psu. Along this segment, ADCP currents were southwestward indicating a reverse of the flow onshore of the NAC (Fig. 3b). At station 86 (Fig. 5a), the θ–S diagram indicates the presence of ''mixed water,'' according to McLellan (1957) and Soule (1951), due to mixing of LCW and slope water, leading to temperatures less than 4°C and salinity between 34.2 and 34.9 psu. Krauss et al. (1990) addressed the question of the origin of this water and found that mixing of NACW and LCW produces a new water mass by cabbeling, which is a considerable source of energy for the NAC all along the continental shelf of the Newfoundland Basin and Flemish Cap up to the NWC.

f. Other fronts from surface signature

Some of the fronts identified along the eastern and southern sections were crossed again when the ship was joining the experimental area from (or to) the Azores. Their position, plotted in Figs. 3a and 3b, helps to complete the synoptic view of the different fronts in the Newfoundland Basin. The surface signatures of three main fronts were detected with the thermosalinograph:

- at 43.6°N, 37.4°W (Fig. 3a), before reaching the western section, a SST front separating 17° from 15°C waters (salinity 36.1–35.5) was associated with a northeastward current. This front was crossed again at the end of the experiment but farther south at 42.6°N, 36.7°W (Fig. 3b), indicating a large variability in its position. Temperature and salinity changes across this front were different (15.7°–13.8°C and 36.1–35.7 psu) because of cooling and evaporation; the current was eastward and reached a maximum speed of 80 cm s^{-1}. This front is thought to be the surface signature of the MWF found at 42°N, 39°W, at the southern end of section south2. Its eastern extension was probably found once more at 44.3°N, 31°W (Fig. 3b), when joining the northern section at the beginning of the second leg. SST dropped from 15° to 13.5°C (SSS from 36 to 35.8 psu) and an eastward current was observed (Fig. 3b).
- Still on the way to the northern section, SST dropped from 12.7° to 11.6°C and SSS from 35.7 and 35.5 psu at 47.7°N, 33.5°W (Fig. 3b); this limit was associated with a southeastward current. This front could have been the continuation of the MAF previously detected during the eastern section.
- At 49.8°N, 34°W (Fig. 3b), a northward current was associated with a SST decrease from 11.6° to 8.5°C and a SSS decrease from 35.5 to 35.2 psu; this front clearly corresponds to the SSAF found on the eastern section.

g. Conclusions

The hydrographic survey allowed us to identify five fronts from the density gradient at 300 m (Fig. 6). The NAC entered the area through the western section, exiting along the northern one and reentering farther east near 49.5°N, 38.5°W. Three fronts were crossed along the eastern boundary: the NSAF, the SSAF, and the MAF from north to south. The signature of the MAF was also found along the southern section. Another front (MWF) was observed at the southernmost point of the survey at 42°N, 39°W.

The surface signature of these dynamical fronts is generally well marked in temperature and density (Fig. 7). This is true for the NAC, NSAF, and SSAF where significant SST gradients were noticed. For the other dynamical fronts, temperature gradients are greater at 300 m than at the surface, but they could still be detected from thermosalinograph data. For this reason, the following sections are devoted to the surface temperatures and currents so that the observations collected on board the ship can be analyzed in the context of a larger synoptic scale.

3. Sea surface temperature

a. SST data

SST analyses were performed every 15 days, using two kinds of data: (i) operational data collected by Vol-

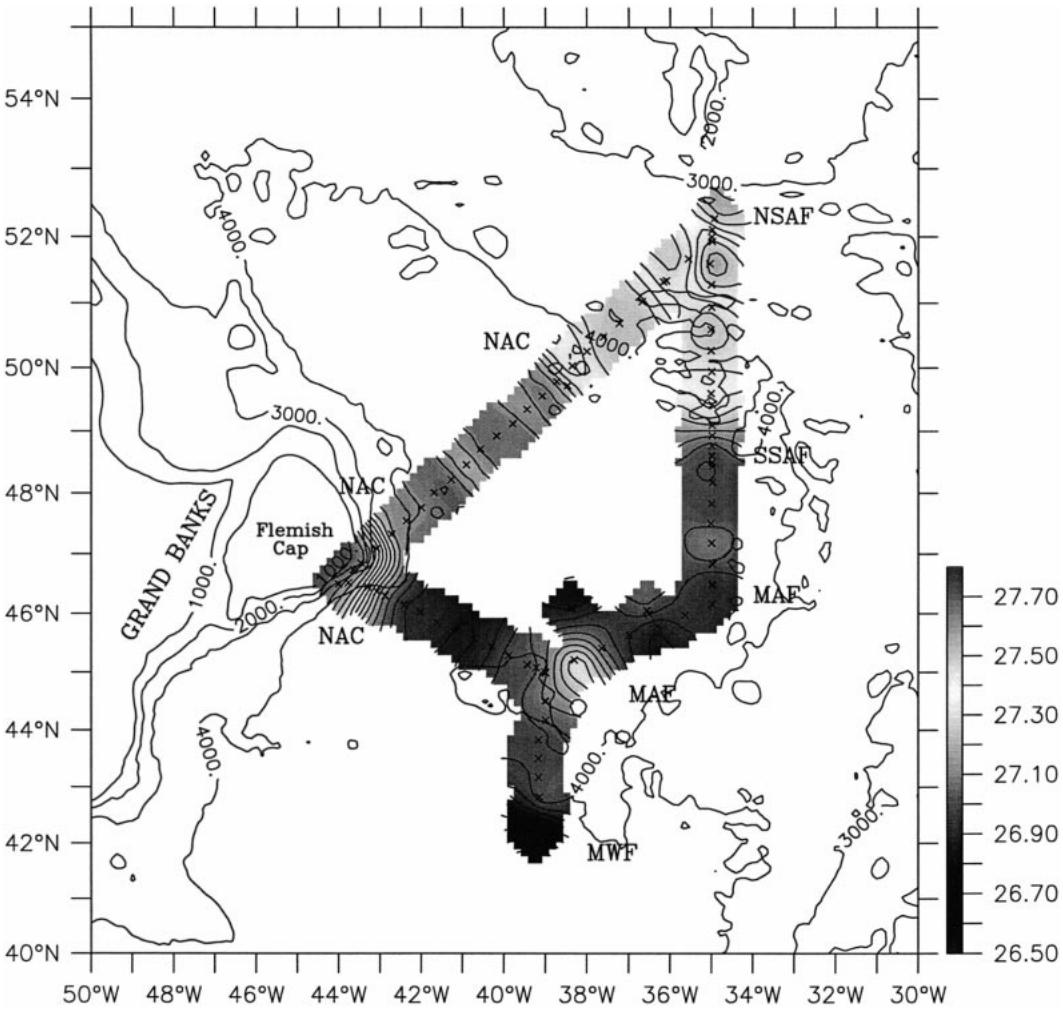

FIG. 6. 300-m deep density along the hydrographic survey. The name and location of the different fronts is reported. The 1000, 2000, 3000, and 4000-m isobaths are superimposed. Crosses indicate the location of CTD casts. SAF stands for the SubArctic Front, NSAF for the North SubArctic Front, SSAF for the South SubArctic Front, MAF for the Mid-Atlantic Front, and MWF for the so-called Mediterranean Water Front.

unteer Observation Ships (VOS) and operational buoys (referred as SMT hereafter), and sent on the Global Telecommunication System (GTS), and (ii) experimental data collected by buoys (CMM hereafter) and three research vessels engaged in the FASTEX experiment (the French ship R/V *Le Suroît*, the Ukrainian ship *Bugaev*, and the American R/V *Knorr*). A total of 9968 data were gathered in the domain 35°N–55°N, 60°–25°W during the two months of the experiment (Fig. 8). Satellite data were not used because of extensive cloud cover during the entire period.

The data from the research vessels are generally of higher quality than data obtained on the GTS. Consequently, merchant marine data were screened before the analysis using two criteria: (i) in the NAC, within the area delimited by a SST gradient of at least 0.02°C/km, data are included directly; and (ii) outside of this area (SST gradient less than 0.02°C/km), data are accepted if the difference with the first guess does not exceed 3°C. Thus strong anomalous deviations from the guess field are eliminated.

b. SST analyses

SST analyses were performed on the domain 35°–55°N, 60°–25°W. This domain is larger than the experimental domain in order to avoid spurious effects from the boundary and is gridded onto 150 × 150 points corresponding to a grid mesh size of about 18 km. This mesh size is a good compromise between numerical cost and the front descriptions obtained. An optimal interpolation algorithm was used (De Mey and Ménard 1989); a brief description is provided in this section.

If Ψ_k^g is the guess field at every grid point k, the optimal interpolation produces an analyzed field Ψ_k^a by a linear combination of $(\Psi_i^o - \Psi_i^g)$ at every observation

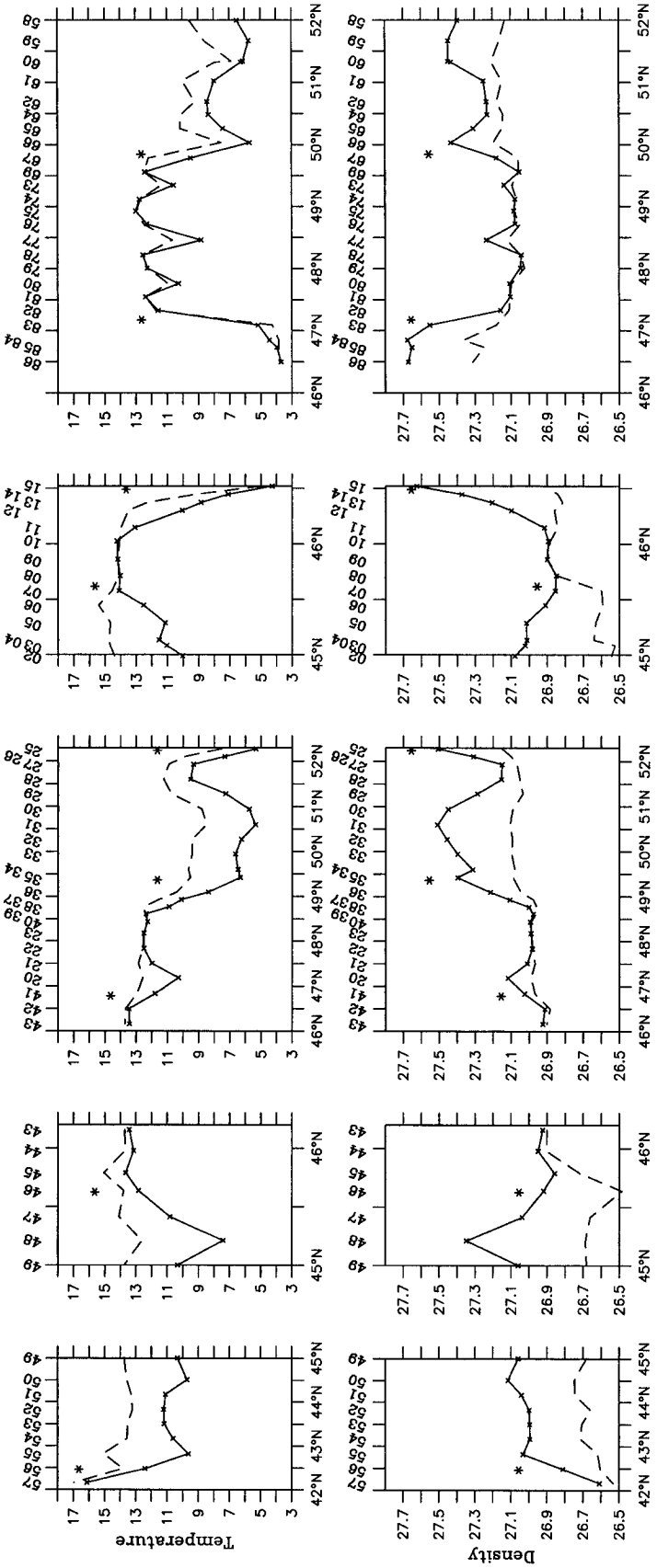

FIG. 7. Same as Fig. 2 but for 300-m temperature (solid line) and sea surface temperature (dashed line) in the top row and potential density anomaly in the bottom row.

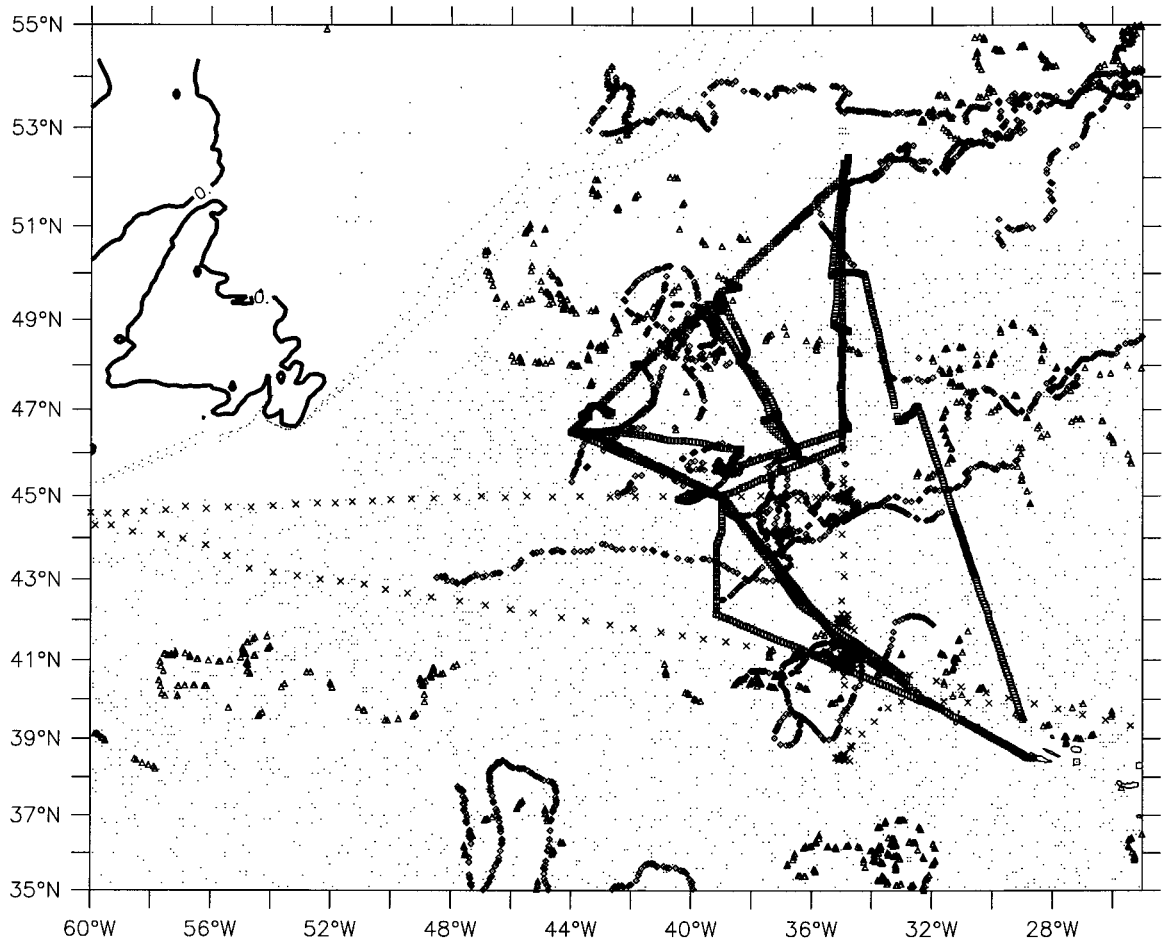

FIG. 8. Location of the 10 000 observations used for the SST analyses during the 2 months of the experiment (Jan–Feb 1997). Crosses represent data from *Bugaev*, squares from R/V *Le Suroît*, diamonds from CMM buoys, triangles from SMT buoys, and points from VOS.

point i (here Ψ_i^o is the observation field and Ψ_i^g the guess at each observation point):

$$\Psi_k^a = \Psi_k^g + \sum_{i=1}^{N_o} \lambda_{ki}(\Psi_i^o - \Psi_i^g),$$

where N_o is the number of observations.

The problem is to compute the coefficients λ_{ki} at every grid point k. They are deduced from the minimization of the analysis error variance σ_a^2 (Rutherford 1972):

$$\frac{\partial \sigma_a^2}{\partial \lambda_{ki}} = f(\lambda_{ki}) = 0 \quad \text{for } i = 1, \cdots, N_o.$$

Using this method, four SST analyses were produced every 15 days and centered on 8 and 24 January and 8 and 23 February to follow the oceanic features, which are known to evolve rapidly in this area (Lazier 1994). Data were included within a temporal radius of 7 days around each central time, and a spatial correlation radius of 150 km. Along- and cross-front horizontal scales were not distinguished because sensitivity tests proved that at scales greater than 100 km the results were not changed. A rather large isotropic correlation radius (150 km) was thus adopted in order to produce an analysis over the whole domain, despite heterogeneous sampling. Note that this scale is in agreement with scales of eddies present in this region (Reynaud et al. 1995). The first analysis was obtained using the SST of the French meteorological weather forecast analysis system (ARPEGE) as a first guess. The other analyses used the previous analysis as guess. The spatial scale implies some smoothing in the analyses, thus a validation with in situ data is presented in the following section.

c. Validation

Figures 9a–e represent the initial guess and the four analyses but only the inner domain 40°–55°N, 50°–30°W is shown for clarity. The front associated with the NAC is present in the ARPEGE first guess but is too smooth in comparison with the four analyses, where horizontal temperature gradients are much stronger and in better agreement with ship data. Table 2 compares the whole SST dataset and the analyzed fields. The analyses are

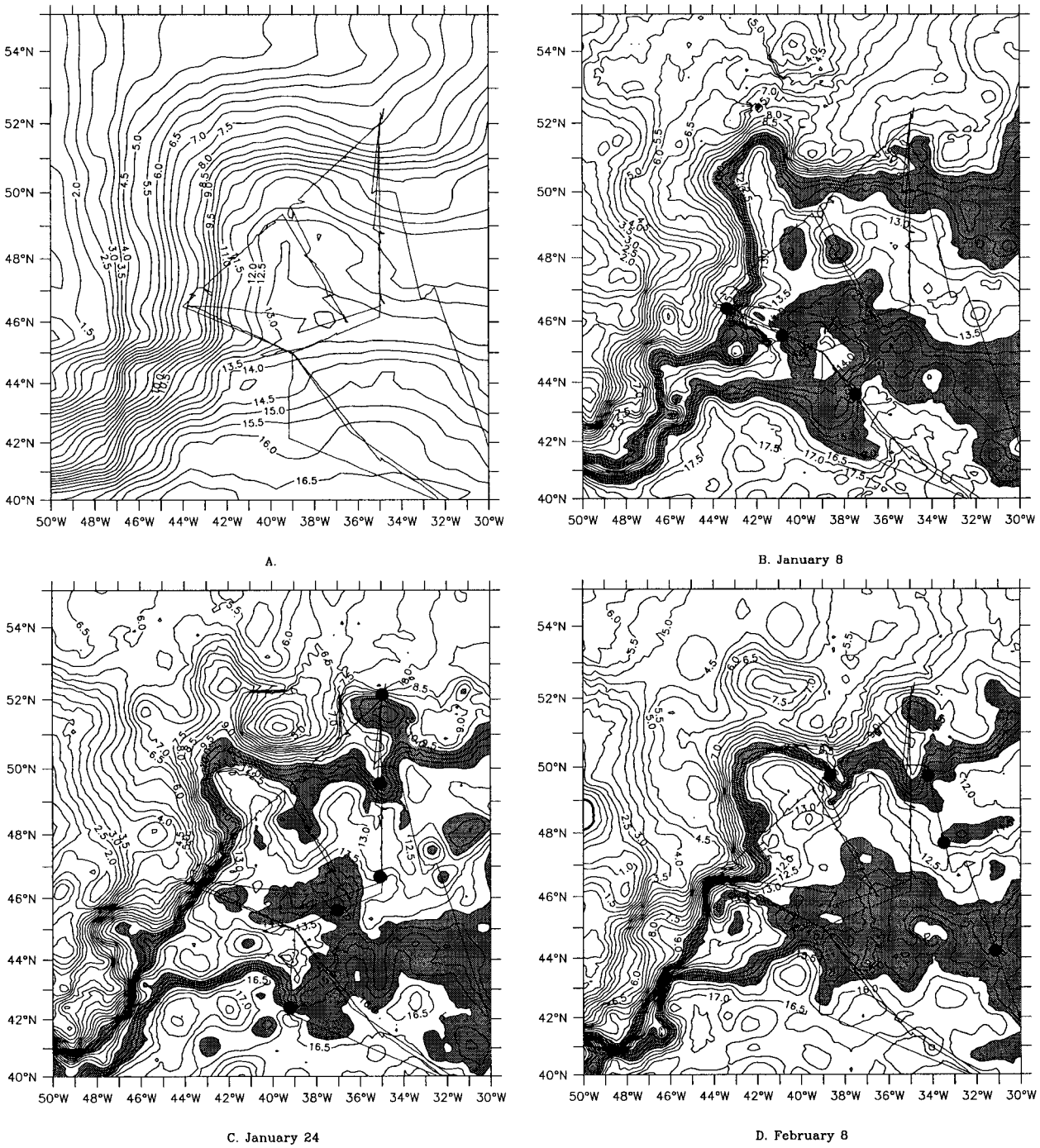

FIG. 9. (a) Initial guess field used for the SST analyses. (b) SST analysis centered on 8 Jan, (c) on 24 Jan, (d) on 8 Feb, and (e) on 23 Feb. The ship trajectory is superimposed. Isolines are every 0.5°C. SST bands highlighted in gray, delimit 10°–12°C and 14°–16°C isotherms on (b) and (c); 9.5°–11.5°C and 13.5°–15.5°C isotherms on (d) and 9°–11°C and 13°–15°C isotherms on (e).

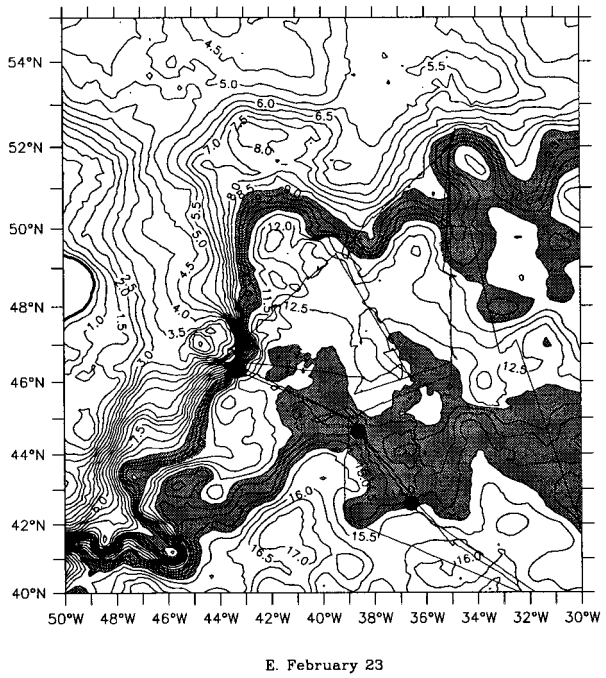

FIG. 9. (*Continued*)

not biased and match well statistically with the observations [correlation 0.98 and root mean square (rms) 0.86°C for the whole dataset]. In comparison, the rms error for the merchant marine data reaches 1.25°C, and ranges between 0.4° and 0.6°C for the other data. The statistics are best when the R/V *Le Suroît*, *Bugaev*, and the SMT and CMM buoy data series are used.

d. Results

Figures 9b–e show the quasi-synoptic surface structures deduced from the objective mapping. In Fig. 9b, the Gulf Stream (GS) enters the southwestern corner (50°W) between 41° and 43°N. It separates warm waters (≥17°C) in the south from cold waters (≤3°C) on its northern side and marks the transition between LCW and NACW. Near 47°W, this front starts a meander northward after its passage over the Newfoundland Rise and near 44°N clearly splits into two branches:

- a southern branch flows eastward after making a large anticyclonic loop. This branch, limited by a sharp gradient is still present at 40°W. East of 40°W, the front is less obvious and makes large meanders and generally flows southeastward before leaving the domain north of the Azores Islands.
- a northern branch flows northeastward with a well-defined temperature gradient. This front corresponds to the NAC and follows particularly well the bathymetry of the Newfoundland plateau up to 47°N (note that the 4°C isotherm roughly corresponds to the 2000-m isobath). At this latitude, which coincides with Flemish Cap, the front turns northwest and then makes a sharp curve toward the east at 51°N, corresponding to the NWC. Downstream from the NWC, the temperature gradients are more diffuse, but a front is still clearly present east of 38°W where it develops large meanders between 50° and 52°N.

TABLE 2. Scores of the SST analyses in comparison with the different datasets collected during the experiment. The number of data is indicated in parenthesis. During the experiment 341 VOS and 51 buoys crossed the area. The few available data (26) from the R/V *Knorr* have been included in the VOS.

Source	Obs. (°C)	Analysis (°C)	Rms (°C)	Correlation
VOS (3858)	13.2	13.2	1.25	0.97
R/V *Le Suroît* (2254)	12.5	12.5	0.56	0.98
R/V *Bugaev* (649)	15.3	15.3	0.45	0.99
SMT buoys (1064)	12.9	12.9	0.45	0.99
CMM buoys (2173)	12.7	12.7	0.5	0.99
Total (9998)	12.7	12.7	0.86	0.98

The positions of the GS, NAC, NWC, the splitting into two branches near 44°N, and the presence of large cyclonic (near 44°N, 42°W) or anticyclonic (near 42°N, 42°W) loops have been described in the literature (see, e.g., the review by Rossby 1996) and are astonishingly well captured in the analyses due to the large amount of data available.

We now consider the temporal evolution depicted by the analyses, from which some interesting features emerge (Figs. 9b–e). First, a global cooling can be seen between 8 January and 23 February due to strong negative surface fluxes at this time of the year (Eymard et al. 1999). Second, there is an intense evolution of meanders and eddies on the 15-day timescale [see, e.g., the formation of the warm eddy at 51°N, 35°W (Figs. 9b–e) or the curvature of the GS around the Newfoundland Ridge in February (Fig. 9e)]. Third, despite these developments, the fronts can be recognized from one analysis to the other and can be considered as permanent at least for the two-month period.

In order to locate the origin of the fronts and their extension throughout the area, two zones of temperature gradients enclosing the GS near 41°N, 50°W were selected. On 8 and 23 January (Figs. 9b and 9c), we chose a temperature range from 14° to 16°C on the anticyclonic side of the GS and from 10° to 12°C on the cyclonic side. These limits were lowered by half a degree on 8 February (Fig. 9d), and one degree on 23 February (Fig. 9e) to take into account the observed SST decrease.

SST bands are not pathways of transport; pathways would be more northerly due to heat loss at the surface. If one considers a parcel of water crossing the domain (nearly 2000 km) at 0.5 m s^{-1}, the order of magnitude of current velocities in the NAC, the time transfer would be nearly 46 days. During this period, a cooling of nearly 1°C was noticed along some sections (see above). If we

take a SST band of 2°C, which is larger than the surface cooling, the band can be used as a good approximation of a transport pathway, provided the parcel of water travels fast enough. In other words, this representation is appropriate for strong currents and strong SST gradients (i.e., for the NAC), perhaps less appropriate for the southern band (which is much larger at the eastern boundary compared with the northern band). Keeping that in mind, we can clearly identify the origin of the main gradients issued from the GS at 50°W, and their eastward extension up to their exit along the 30°W border.

The northern band delimits the warm side of the NAC and is a good indicator of the SSAF in the eastern part of the domain. This band stays narrow up to the NWC as long as it stays locked to the Newfoundland plateau. Downstream from the NWC, meanders develop with a rather large north to south extension. Note that the position of the SSAF and NSAF identified along the eastern section of the survey is in good agreement with the SST analyses and the presence of meanders are clearly confirmed.

The southern temperature band marks the position of the front found near 42°N, 39°W (Fig. 9c). Farther east, this temperature band widens and extends from 42° to 47°N. Although its shape and evolution are quite complex, and surface heat loss important, this band can be considered as enclosing waters between MWF and MAF. We infer that two branches split in the area 43°–44°N, 38°–37°W: the northern branch supplying the MAF, with a mushroom shape extension inside the investigated trapezoid up to 47°N (cf. Figs. 6 and 9c) and the eastern branch that continues eastward, north of the Azores Islands. Note that the eastern extensions of the MAF and MWF were identified respectively at 47.7°N and near 44°N along the easternmost trajectory of the ship (Figs. 3b and 9d), that is, higher in latitude than indicated by the SST band. This shift clearly indicates the limits of mixing the SST bands with the transport pathways.

The presence of a cold SST near 45°N, 39°W (Figs. 9b and 9c) is associated with an eddy. At this point, we identified SAIW outcropping up to 200 m (station 48, Figs. 2, 5d, and 6). This eddy is thought to have been detached previously from the NAC and to have been advected to the east. From a large historical hydrographic database (1910–88), Kearns and Rossby (1998) identified the most probable location of the NAC. They found that the NAC could migrate from the continental margin almost to the Milne Seamounts with a probability less than 5%. Such an event probably occurred shortly before the experiment, leaving as far as 39°W a cold cyclonic eddy. Note that its surface signature vanishes in February (Figs. 9d and 9e).

In conclusion, we note a significant measure of realism in these analyses in being able to retrieve some classical features observed in the literature; there is a good agreement with observations of the CTD array and good temporal continuity between the four analyses; finally, it is possible to locate the different fronts identified from the CTD array throughout the whole basin. However, some limits were identified in locating fronts only from SST maps. This is the reason why altimetry is now used to derive a complementary description of the circulation.

4. The circulation deduced from altimetry

a. Altimetry analysis

The high space–time resolution of satellite altimetry allows a complementary description of the circulation in the Newfoundland Basin. Using sea surface height (SSH) provided by both TOPEX/Poseidon (T/P) and *ERS-2* satellites we can resolve the mesoscale circulation (Koblinsky et al. 1992; Blayo et al. 1997; Le Traon and Dibarboure 1999). An accurate synoptic description of sea level variations can be obtained by merging these two sets of satellite data using mapping techniques (Hernandez et al. 1995).

We use the SSH of T/P reprocessed merged GDRs (GDR-M Version C), distributed by AVISO (AVISO 1996), and *ERS-2* OPRs, distributed by CERSAT (CERSAT 1994, 1996) from December 1996 to March 1997. In order to combine these, the 9.95-day-repeat T/P and 35-day-repeat *ERS-2* data need to be homogeneous and intercalibrated. The CSR3.0 tidal model (Eanes and Bettadpur 1995) was used for both missions. For more details on the corrections applied to T/P and *ERS-2* SSH data, the reader is referred to Le Traon and Ogor (1998). Intercalibrated datasets are then obtained by performing a global crossover adjustment of the *ERS-2* orbits, using the more precise T/P data as a reference (Le Traon and Ogor 1998).

Since the marine geoid is not accurate at small spatial scales, SSH along each satellite track are referenced to a mean profile, to provide along-track sea level anomalies (SLA) using the conventional repeat-track analysis (e.g., Cheney et al. 1983).

In this analysis, both T/P and *ERS-2* SLA are referenced to the same mean ocean surface, which is calculated from combined T/P and *ERS-1* data from January 1993 to January 1996, using the techniques described by Hernandez (1999, submitted *J. Atmos. Oceanic Technol.*). This technique has the advantage of minimizing the seasonal and interannual aliasing in the mean profile. To reduce measurement noise, SLA data are along-track filtered using a linear Lanczos low-pass filter with a 70-km cutoff. Maps of SLA, combining T/P and *ERS-2* data have been calculated at the same time and on the same grid as the SST analysis. The mapping method is a suboptimal space–time objective analysis (Bretherton et al. 1976) that takes into account along-track correlated errors. For a more detailed description of this mapping technique, the reader is referred to Hernandez et al. (1995) and Le Traon et al. (1998). More specifically, the analysis has been performed using space

(isotropic) and time correlation functions with a 120-km and 15-day zero crossing, intending to represent the typical scales of the mesoscale circulation. Measurement noise was set to 2 cm for T/P and 3 cm for *ERS-2*, and large wavelength errors estimated at 3 cm for T/P and 4 cm for *ERS-2* (note that the adjustment of *ERS-2* SSH data to T/P reduces the long wavelength error levels).

Because SLA are obtained by removing the mean sea level, a climatological background dynamic height anomaly (DHA) has been added to reconstruct the mean flow. This procedure has already been developed by Willebrand et al. (1990) in the GS extension. The background DHA was computed from the Kearns and Rossby (1999, submitted to *J. Geophys. Res.*) high-resolution climatology of the waters in the Newfoundland Basin, using specific volume anomaly levels between $\delta = -43.7 \times 10^{-8}$ m^3 kg^{-1} and $\delta = 34.3 \times 10^{-8}$ m^3 kg^{-1}. The DHA was added to the satellite SLA, after interpolation on the same grid. The choice of specific volume anomaly bottom level ($\delta = -43.7 \times 10^{-8}$ m^3 kg^{-1}) lies on average close to 2000 m in the plain between the Newfoundland Plateau and the Mid-Atlantic Ridge. When the upper level ($\delta = 34.3 \times 10^{-8}$ m^3 kg^{-1}) does not outcrop, its depth lies on average near 300 m and from the surface down to this depth, δ has been supposed constant. This climatology has been chosen because the quasi-permanent path of the NAC is well resolved, a feature that altimetry fails to reconstruct.

b. Validation

In order to check the representativity of satellite data, we first compare satellite SLA with in situ DHA along the hydrographic sections. Then, currents deduced from altimetry are compared with ADCP data.

1) DYNAMIC HEIGHT ANOMALIES AGAINST IN SITU DATA

To better compare the in situ dynamic height with the sea level measured by altimetry, SLA has been estimated at the same time and position as each hydrographic cast. A technique similar to the SLA mapping procedure was performed but, instead of estimating SLA in a regular grid at a given time, altimetric data were selected for estimating SLA at each hydrographic station and then added to the climatology DHA. The comparison is plotted in Fig. 10. The altimeter signal agrees quite well with in situ observations both for large- and small-scale structures. Rms for the northern, eastern, southern, and western sections are respectively 9.3 cm, 5.9 cm, 11.5 cm, and 8.4 cm and correlations 88%, 93%, 89%, and 95%.

The best performance is obtained along the eastern section because the climatological background has a relatively well positioned north to south trend due to its quasi-permanent structure. Less good scores are registered for the northern section due to the presence of small but energetic eddies or meanders.

2) ALTIMETRIC CURRENT AGAINST ADCP

Geostrophic currents were deduced from satellite altimetry and plotted along with ADCP measurements in Fig. 11. A large part of the domain (from 52° to 42°N, that was covered by the ship from 25 to 31 January) is presented and includes the eastern and the two southern sections. ADCP data have been subsampled and are shown every 10 km. Currents deduced from SLA and climatology were interpolated at the ship position from the 24 January analysis. The good comparison suggests that the ageostrophic component of the current is weak in the ADCP data. Mixed layer depths were generally deep during this period (200–300 m on average), and the ADCP data represent the layer from 0 to 150 m. This means that, at first order, the Ekman component can be considered as negligible in the data. An estimate of the Ekman current was still performed by running a one-dimensional model, initialized with CTD profiles collected along the western section and forced with atmospheric fluxes derived from the European Center for Medium-Range Weather Forecasts (ECMWF) model: the Ekman transport (integral of the current down to 150 m, the depth limit of the ADCP) reached peak values of 0.07 m s^{-1}, with a mean less than 0.03 m s^{-1}. It would therefore appear that ADCP currents are essentially geostrophic.

From Fig. 11, the vector correlation is 0.79 and the correlation angle (ratio between the rotation and the stretching correlation coefficients, knowing that the best correlation is obtained with an angle of 0°) is 16°, meaning that the statistical comparison between currents is satisfactory. Except locally, the position and orientation of the main frontal currents are qualitatively well reconstructed. Satellite-derived current velocities are weaker than observed by 0.07 m s^{-1} on average. Consequently this validation indicates that the main satellite currents can be used to extend the observations along the ship survey to the whole domain with rather good confidence.

c. Dynamic height anomalies and currents

Figure 12a displays one map (23 February) of SLA (plus climatological DHA) and Figs. 12b–e the currents deduced from SLA with temperature bands of Figs. 9b–e superimposed. Eddies dominate both the DHA and the current fields and have spatial scales of some hundreds of kilometers. The amplitudes of the eddy field reach values up to 0.60 dyn m (Fig. 12a). The highest values are located in the GS area and offshore of the NAC. SLA decreases quite uniformly eastward and drops sharply on its inshore side. The presence of stronger eddies downstream from the GS and along the core of the NAC reflects the EKE revealed by drifter studies

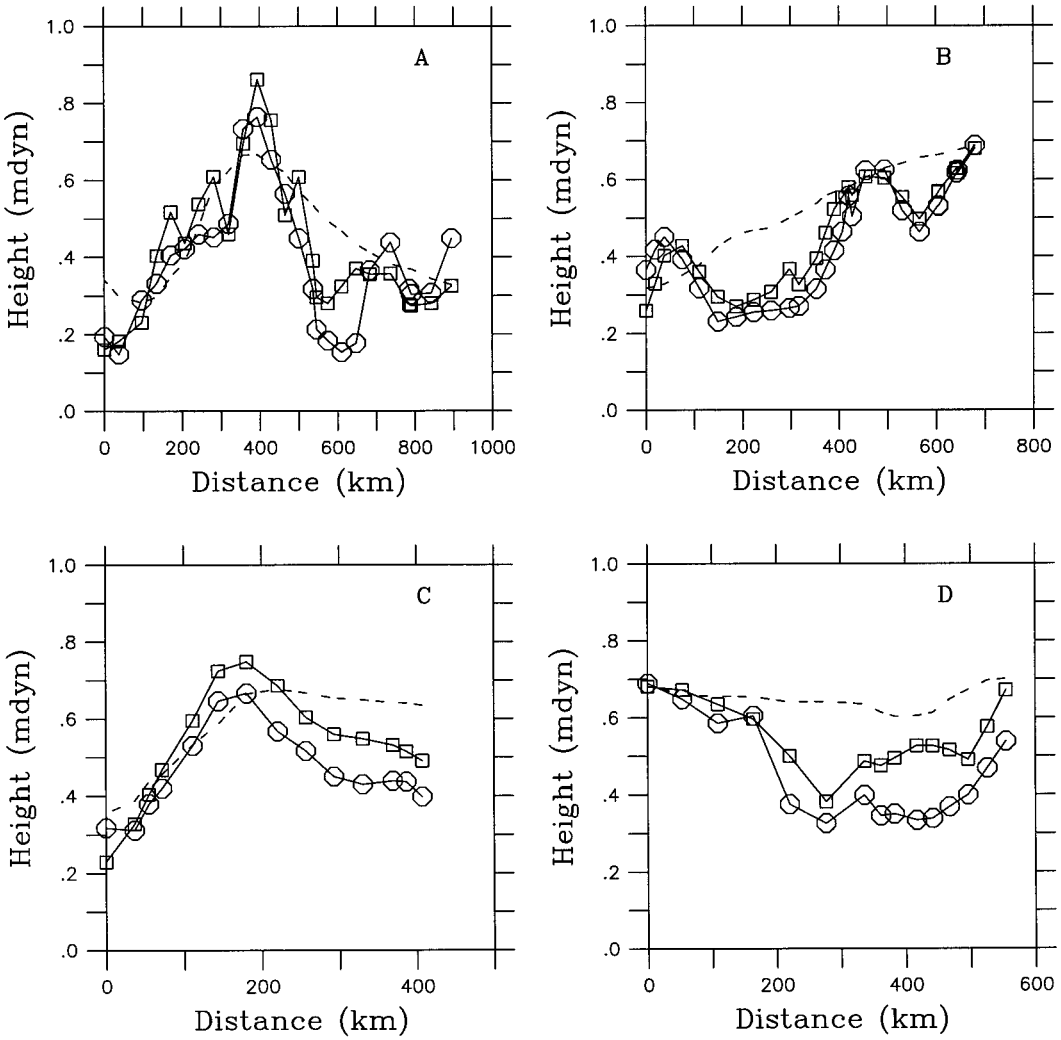

FIG. 10. Dynamic topography (in mdyn) from hydrographic data (squares) and surface topography from altimetry plus climatology (circles). Climatological topography is indicated by a dashed line. (a) Along the northern section (from west to east), (b) eastern (from north to south), (c) western (from west to east), and (d) the two southern (from north to south) sections.

(Krauss and Käse 1984; Rossby 1996) or deduced from Geosat data by Le Traon et al. (1990).

Although the circulation offshore of the NAC is complex and highly nonstationary, some features are permanent enough during 2 months to be mentioned. Anticyclonic eddies are present between 41° and 43°N, 46° and 40°W (Figs. 12a–e). This region corresponds to the warmest waters of our area (Figs. 9b–e) and is known as the area of residence of the famous Mann Eddy (Mann 1967). North of these eddies, a large cyclonic trough extends between the Newfoundland Seamounts and the Milne Seamounts near 44°N, 42°W, where at this precise location Rossby (1996) identified a semipermanent trough. Northeast of Flemish Cap, there is evidence of a recirculation area with energetic and quickly evolving eddies, as noted by Käse and Krauss (1996).

The current analyses are not only in good agreement with what is known from the circulation, but there is also a good agreement between the position of strong currents and the position of fronts identified with the CTD array (represented as black dots in Figs. 12a–e), meaning that the pathways of transports can easily be tracked throughout the basin. Moreover comparison of pathways of currents and SST bands shows that several features are present in both analyses. The temperature band that marks the position of the NAC along the Newfoundland plateau and of the SSAF eastward is in good correspondence with the strong currents defining these dynamical fronts. Strong currents are clearly associated with the water path defined by the 14°–16°C isotherms along 43°N. Large meanders along 43°N, and along the NSAF and SSAF east of 39°W, are visible in both analyses and generally fairly close to each other. Eddies identified from hydrographic measurements are present

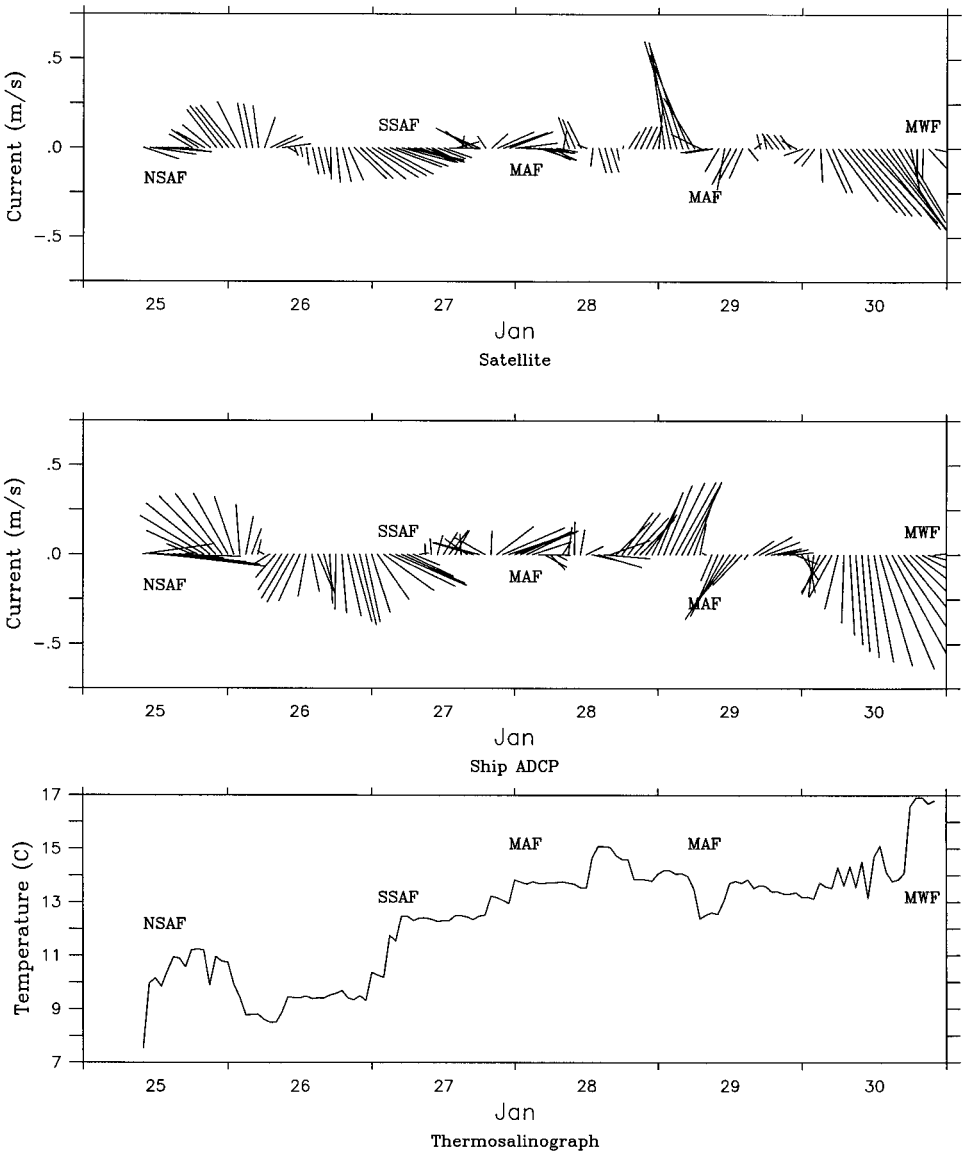

FIG. 11. (top) Satellite-derived currents, (middle) ADCP current data, and (bottom) SST from the thermosalinograph along the ship track from 25 to 31 Jan. This trajectory includes the eastern section and the two southern sections from 52° to 42°N. The locations of the NSAF, SSAF, MAF, and MWF are indicated. ADCP data are plotted every 10 km for clarity.

both in the current and SST maps: for example, the anticyclonic eddy at 48°N, 40°W and the cyclonic eddy located 45°N, 39°W in January (Figs. 12b,c), which vanishes in February (Figs. 12d,e).

There are also some differences where strong currents do not coincide with SST fronts. The NWC does not extend farther north than 51°N in temperature but eddies are clearly present up to 53°N [this feature has already been observed from the buoy network by H. T. Rossby (1999, personal communication)]. Along 43°N, or in the meanders nears 51°N, a phase shift is nearly always present between the highly turbulent flow and the SST field. We do not think that these features are an artefact of the analysis but rather that they correspond to shifts that exist between a highly turbulent current field and a scalar field like temperature. Current (and SSH) fields exhibit an eddy rich nature that is less apparent in SST fields. Because currents frequently appear to be directed across the gradient, horizontal advection must be an important local process controlling the SST evolution in this area. Despite these differences, which more or less reflect the physics of the flow, both temperature and current contribute to give a realistic representation of the circulation in the Newfoundland Basin.

In the next section, mass transports are calculated from the hydrographic survey and are superimposed on

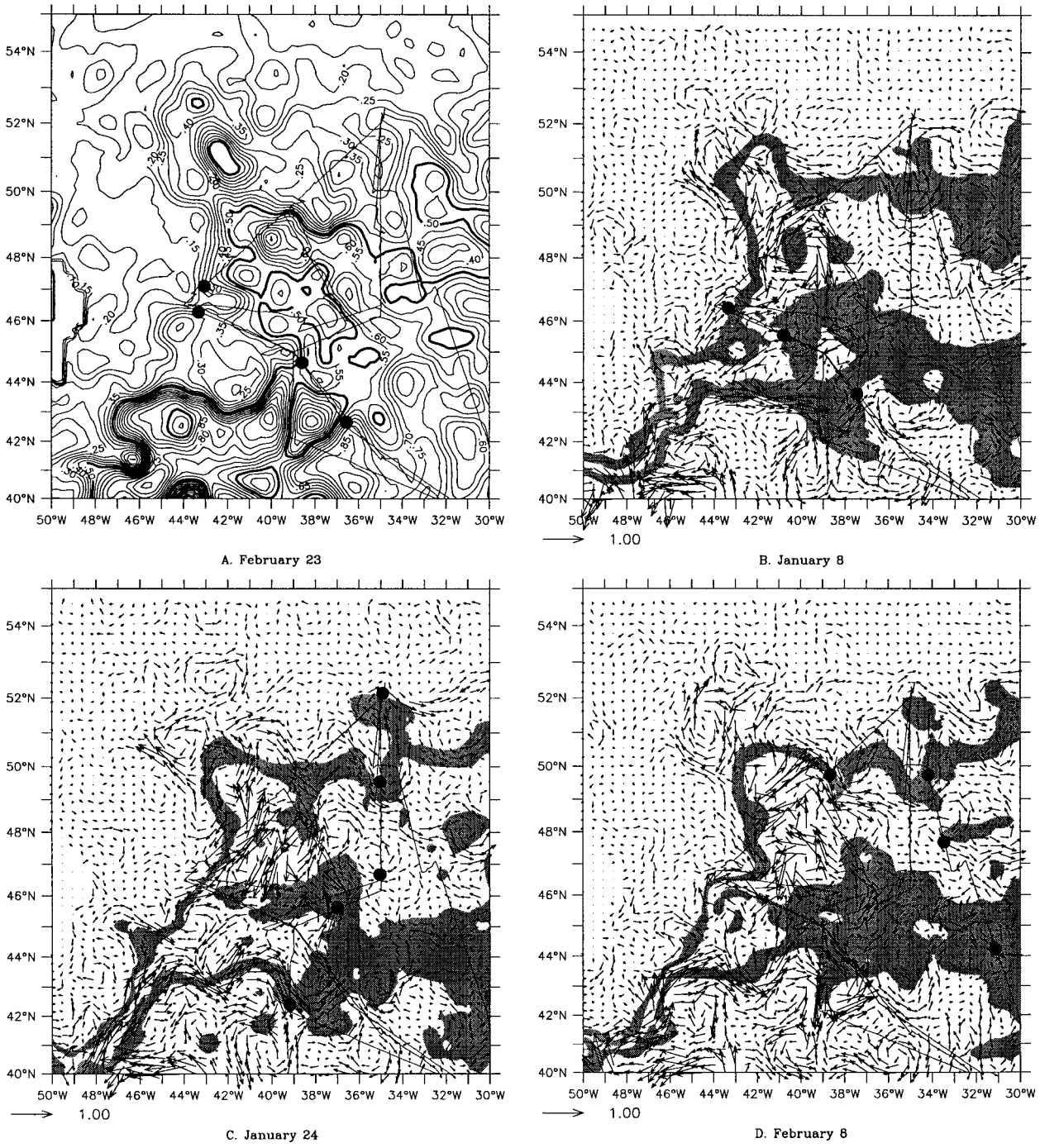

FIG. 12. (a) Composite sea surface height anomaly from TOPEX/Poseidon and *ERS-2* combined with the dynamic topography derived from the Kearns and Rossby (1999, submitted to *J. Geophys. Res.*) climatology for the analysis of 23 February. Contour interval is 5 cm. (b) Surface currents calculated with composite sea surface height anomaly from TOPEX/Poseidon and *ERS-2* and the mean dynamic topography derived from the Kearns and Rossby's climatology on 8 January. (c) 24 January. (d) 8 February. (e) 23 February. Temperature bands from Figs. 9b–e superimposed. Blacks dots indicate the position of the fronts detected from the hydrographic survey or from the thermosalinograph data.

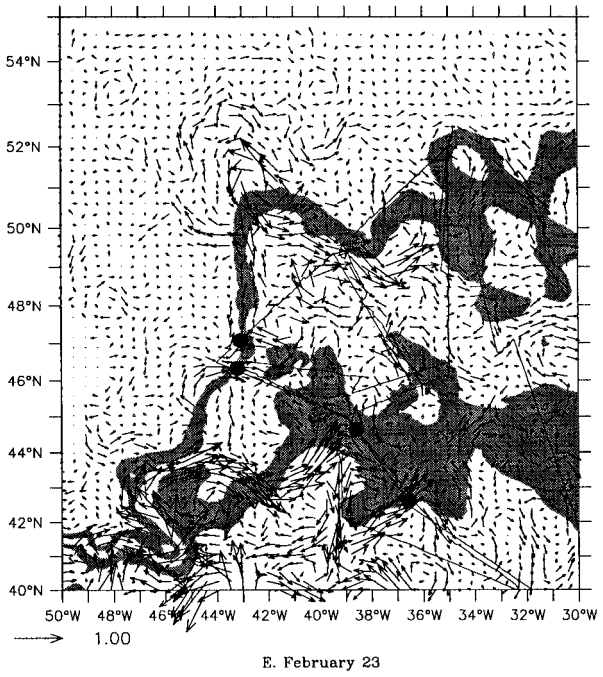

FIG. 12. (*Continued*)

the composite surface current field to derive a mean circulation pattern.

5. Mass transports

a. Balance

All the transports have been computed from the CTD casts using the classical method described by Fofonoff (1962). The final balance of transport across the trapezoid is given in Table 3, where two reference depths are considered: 1800 dbar and 1500 dbar. An inflow of 26.6 Sv (24.8 Sv at 1500 dbar) (Sv $\equiv 10^6$ m^3 s^{-1}) enters the box from the west and the south and 30.8 Sv (28.6 Sv) leaves via the eastern and northern boundaries. A residual of 4.2 Sv is obtained in the box, nearly the same (3.8 Sv) when the reference level is 1500 dbar. This residual is the same order of magnitude as that obtained by Krauss et al. (1990) for a similar CTD pattern across the branching of the GS southeast of the Grand Banks. These authors found that the residual could be lowered when taking a reference level based on a $\sigma_\theta = 27.83$ surface. This test could not be performed because our profiles were limited to 2000 m. However, the western section was covered twice during the experiment: at the beginning of January and at the end of February. At the end of February, the transport was 16.8 Sv along this section, higher than in January (12.7 Sv). The difference (4.1 Sv) being the same order of magnitude as the residual, we prefer to interpret this residual as not crucially dependent of the reference level but rather to the nonstationarities of the eddy field and to the nonsynopticity of the survey for which more than one month was necessary to complete the four sections.

TABLE 3. Mass transport (in Sv) along the different sections of the hydrographic survey and computed with two reference levels. Positive values indicate transport out of the trapezoid.

Layer	Western section	Southern section	Eastern section	Northern section	Sum
15–1500 dbar	−11.71	−13.10	23.30	5.31	3.80
15–1800 dbar	−12.73	−13.88	25.13	5.73	4.25

b. Detailed transports

The altimetry data, the SST analyses, and the hydrography allow a more meaningful transport interpretation along the different branches of the flow. Each pair of stations was systematically used to calculate the transports not only along each section but also between points on different sections, with the requirement that their time difference is limited to a maximum of 10–15 days.

Given that the currents are in close agreement with the CTD array, the current maps were used to identify the most probable direction of the flow inside the array, allowing us to eliminate unrealistic solutions. The composite surface velocity map (Fig. 13), obtained as the average of the four satellite maps (Figs. 12b–e), is a summary of this approach and is used to devise a consistent interpretation of the baroclinic transport.

A problem identified is the important time variability. The 4.1 Sv difference along the western section between January and February was already mentioned. Another example is the westward 17 Sv transport obtained between stations 2 and 16 (separated by 5 days) and an eastward 1 Sv transport estimated across the same line from the balance obtained from stations 16, 18, 43, and 49 (Fig. 1). This difference is due to the presence of the strong evolving eddy at 45°N, 39°W identified in the CTD survey, on satellite maps, and the SST analyses. Finally some choices were made to be coherent. For instance, the transport in the NAC was calculated twice: 32 Sv between stations 10 and 15 and 15 Sv between stations 81 and 86. We chose 15 Sv as final solution and included a recirculation area inside the trapezoid to take into account the large variability in this area.

The following circulation pattern can thus be deduced (Fig. 13): the NAC transports 15 Sv near 47°N, 43°W when crossing the western end of the northern section and transports 12 Sv when it reenters the trapezoid at 50°N, 39°W, loosing 3 Sv during its northern excursion. Near 49°N, 38°W the NAC splits into two branches: one transports 8 Sv and the other continues northeastward with 4 Sv while loosing 2 Sv before reentering the trapezoid near 51°N, 36°W. Three branches converge at 49°N, 35°W as the SSAF (12 Sv). The current associated with the NSAF transports 7 Sv. The MAF comes from

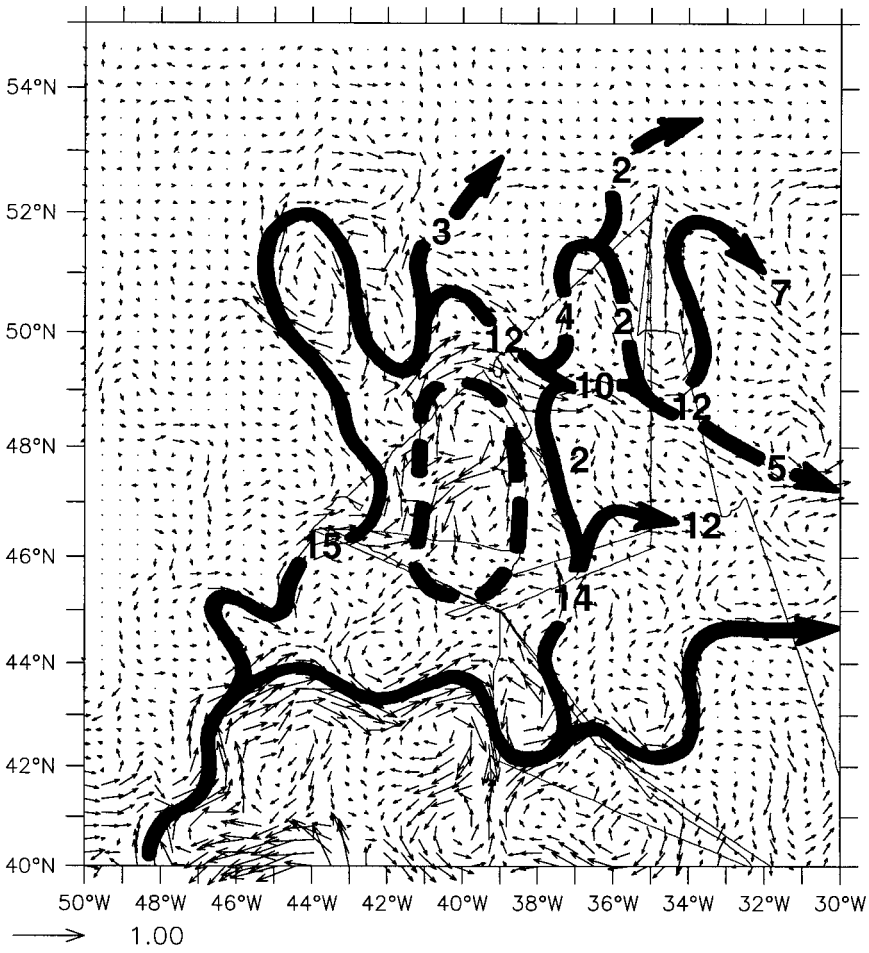

FIG. 13. Currents calculated by averaging the four fields of Figs. 12b–e. Transports (in Sv) were calculated from the CTD array and the main branches of the flow were deduced from Figs. 9 and 12. The dashed line encloses the recirculation area (see text).

a splitting of the current near 43°N, 38°W; it enters the sampled zone with 14 Sv and retroflects near 47°N before crossing 35°W with 12 Sv.

The transport associated with the southernmost branch of the flow was measured at 15 Sv at 42°N, 39°W. This transport is largely underestimated because the southernmost section was stopped too far north. The main reason is that this flow branches northward with 14 Sv near 43°N, 38°W, leaving a residual (1 Sv) which is obviously too low for the downstream southeastward flow. On the assumption that the NAC transports 45 Sv at 42°N (Kearns and Rossby 1999, submitted to *J. Geophys. Res.*) and 15 Sv flow northward (this study), 30 Sv would flow eastward, meaning that our transport (15 Sv) would be underestimated by about 15 Sv along this branch.

Inside the NWC, we conclude that a closed recirculating area must exist (dashed line in Fig. 13). A similar result was previously suggested by Käse and Krauss (1996). In this area, the exchange of transport between the system of eddies inside the NWC (Fig. 2, column 5 and Figs. 12b–e) and the surrounding flow was less than 0.5 Sv. This recirculation gyre was observed with a relatively north to south elongation during January but during February it literally burst out into several cyclonic and anticyclonic eddies (Figs. 12b–e). These eddies were very energetic and their transports were measured as high as 27 Sv. The recirculation flow was crossed in January along the western section (17 Sv) and cumulated with the NAC, gave a total of 32 Sv.

Our transport by the NAC at 47°N, 43°W is compatible with previous measurements between 15 and 20 Sv of Mann (1967), Clarke et al. (1980), Schmitz (1985), but less than 24 Sv of Carr et al. (1997) climatology at 47°N. The transport in the recirculation gyre of the Newfoundland Basin is the same order of magnitude in comparison to 18 Sv found by Clarke et al. (1980) or 15–20 Sv by Schmitz (1985). Along 35°W, our 26 Sv escaping toward the Mid-Atlantic Ridge is comparable with the 23 Sv reported by Käse and Krauss (1996). However, a more detailed comparison should be made using only the wintertime transport. Up to now estimates

from in situ data are scarce and comparisons with climatological studies difficult because they fail to retrieve the branching of the NAC (Kearns and Rossby 1999, submitted to *J. Geophys. Res.*).

6. Conclusions

A trapezoidal hydrographic survey has been conducted in the Newfoundland Basin during January and February 1997. To our knowledge, this survey is the first systematic midwinter investigation of this area.

The ship's trajectory was chosen so as to cross the main current systems of this complex and highly turbulent region. Along the western section, the North Atlantic Current (NAC) was found at 46°N, 43°W, associated with a sharp temperature gradient separating 5°C from 13°C waters. Three surface fronts were observed along the eastern section at 35°W: the North Subarctic Front (NSAF) at 52°N, the South Subarctic Front (SSAF) at 49°N, and the Mid-Atlantic Front (MAF) at 47°N. The so-called Mediterranean Water Front (MWF) was found at 42°N, 39°W and its surface signature was also recognized farther east at 44°N, 31°W.

In addition to this unique hydrographic dataset, we have also developed a new methodology based on surface data analyses in order to monitor and interpret the winter circulation in this area. The surface data analyses have been successfully tested on the hydrographic dataset. The different steps of this approach are summarized here. Due to the deep winter mixed layers (nearly 300 m), SST fronts were a good signature of the dynamical fronts. SST analyses were produced every 15 days (a good temporal scale for the high variability of mesoscale features in this basin), using all available data on the GTS plus extra drifting buoys and research vessel data. These fine-resolution maps provided a realistic picture of the SST fronts observed in the survey. The common origin of these fronts has also been identified as coming from the Gulf Stream area, provided that the SST gradients (or associated currents) are strong enough.

Altimetric data, combined with a fine-resolution climatology was then used to produce analyses at the same resolution as the SST analyses. Altimetric sea level anomalies and currents were validated against CTD height anomalies and proved that currents could be used to identify the main branches of the NAC system. Good agreement was obtained between SST and satellite current maps. Observations collected during the hydrographic survey were thus put into a broader context, which enabled a synoptic description of the surface circulation and its evolution during the two months of the experiment. Transports were calculated from CTD stations, and the combined SST and current analyses allowed us to reconstruct all the pathways of transport inside this area in a coherent framework.

The circulation pattern deduced from these combined data reveals the presence of an intense recirculating gyre offshore from the NAC from 46° to 49°N and 39° to 41°W. In this area, an astonishing 100-km-wide eddy with a mixed layer 800 m deep was present and its transport was 27 Sv. The NAC was found to transport 15 Sv at 47°N, 43°W, a value comparable with previous estimates. Downstream from the Northwest Corner, the NAC widens, and its transport decreased to 12 Sv at 50°N, 39°W. The NAC was observed to burst into several branches east of 40°W, in an intricate system of loops and meanders (e.g., near 49°N, 38°W and 43°N, 38°W). Among these branches, the South Subarctic Front had a transport of 12 Sv and the Mid-Atlantic Front 12 Sv.

Further investigation into the complex circulation of the Newfoundland Basin could now be undertaken following the methodology proposed in this paper. By using routinely available surface data (from volunteer observation ships, buoys, and satellite SST and SSH), circulation patterns could be reconstructed and the transport along specific currents/fronts evaluated from mooring arrays or tomography techniques.

Acknowledgments. We should like to acknowledge the officers and crew of the R/V *Le Suroît* and the scientific staff of LPCM (Laboratoire de Physique et Chimie Marines), CNRM (Centre National de Recherches Météorologiques), CETP (Centre d'Etudes Terrestres et Planétaires), ETH (Eidgenössische Technische Hochschule, Zürich), and NCAR (National Center of Atmospheric Research), who all struggled under very difficult conditions to acquire the data presented in this paper. We are also grateful to the staff of the FASTEX operational center of Shannon (Ireland) for their meteorological support. We thank Jean Raunet for the high quality data acquisition in very harsh weather conditions, Gilles Reverdin for providing us sea surface data of the Godafoss trade ship, and E. J. Kearns for his permission to use his high-resolution climatology. We are grateful to H. T. Rossby for his very constructive comments and an anonymous reviewer who both contributed to really improve the manuscript. Special thanks to Rosemary Morrow for her help in correcting our English and Youcef Amar for drawing the figures. This work has been supported by the PATOM of the INSU–CNRS, Météo-France, and SHOM.

REFERENCES

Arhan, M., 1990: The North Atlantic Current and Subarctic Intermediate Water. *J. Mar. Res.*, **48,** 109–144.

——, and B. King, 1995: Lateral mixing of the Mediterranean Water in the eastern North Atlantic. *J. Mar. Res.*, **53** (6), 865–895.

——, A. Colin de Verdiere, and H. Mercier, 1989: Direct observations of the mean circulation at 48°N in the Atlantic Ocean. *J. Phys. Oceanogr.,* **19,** 161–181.

AVISO, 1996: Archiving, validation, and interpretation of satellite oceanographic data, AVISO Handbook for merged TOPEX/Poseidon products. 3d ed. Handb. AVI-NT-02-101-CN, Toulouse, France, 201 pp. [Available from CNES, 18 Avenue Edouart Belin, 31057 Toulouse Cedex, France.]

Belkin, I. M., and S. Levitus, 1996: Temporal variability of the Subarctic Front near the Charlie-Gibbs Fracture Zone. *J. Geophys. Res.*, **101** (C12), 28 317–28 324.

Blayo, E., T. Mailly, B. Barnier, P. Brasseur, C. Le Provost, J. M. Molines, and J. Verron, 1997: Complementarity of *ERS-1* and TOPEX/Poseidon altimeter data in estimating the ocean circulation: Assimilation into a model of the North Atlantic. *J. Geophys. Res.*, **102,** 18 573–18 584.

Bretherton, F., R. Davis, and C. Fandry, 1976: A technique for objective analysis and design of oceanographic experiments applied to MODE-73. *Deep-Sea Res.*, **23,** 559–582.

Brügge, B., 1995: Near-surface mean circulation and kinetic energy in the central North Atlantic from drifter data. *J. Geophys. Res.*, **100** (C10), 20 543–20 554.

Carr, M. E., E. J. Kearns, and H. T. Rossby, 1997: Isopycnal RAFOS floats as roving hydrographers in the North Atlantic region. *Geophys. Res. Lett.*, **24,** 551–554.

CERSAT, 1994: Centre ERS d'Archivage et de Traitement: *ERS-1* altimeter products user manual. Handb. C1-EX-MUT-A21.01-CN, Brest, France, 52 pp. [Available from CERSAT-IFREMER Technopole Brest-Iroise, BP 70, 29200 Plouzané, France.]

——, 1996: Centre ERS d'Archivage et de Traitement: Altimeter and microwave radiometer ERS products user manual. Handb. C2-MUT-A-01-IF, Brest, France, 136 pp. [Available from CERSAT-IFREMER Technopole Brest-Iroise, BP 70, 29200 Plouzané, France.]

Cheney, R. E., J. G. Marsh, and B. D. Beckley, 1983: Global mesoscale variability from collinear tracks of Seasat altimeter data. *J. Geophys. Res.*, **88** (C7), 4343–4354.

Clarke, R., H. Hill, R. Reiniger, and B. Warren, 1980: Current system south and east of the Grand Banks of Newfoundland. *J. Phys. Oceanogr.*, **10,** 25–65.

Colin de Verdière, A., H. Mercier, and M. Arhan, 1989: Mesoscale variability transition from the western to eastern Atlantic along 48°N. *J. Phys. Oceanogr.*, **19,** 1149–1170.

De Mey, P., and Y. Ménard, 1989: Synoptic analysis and dynamical adjustment of GOES 3 and Seasat altimeter eddy fields in the northwest Atlantic. *J. Geophys. Res.*, **94,** 6221–6231.

Dietrich, G., K. Kalle, W. Krauss, and G. Siedler, 1980: *General Oceanography: An Introduction.* 2d ed. John Wiley and Sons, 626 pp.

Eanes, R. J., and S. V. Bettadpur, 1995: The CSR3.0 Global Ocean Tide Model. Center For Space Research Report CSR-TM-95-06, University of Texas, Austin, TX.

Eymard, L., and Coauthors, 1999: Surface fluxes in the North Atlantic Current during the CATCH/FASTEX experiment. *Quart. J. Roy. Meteor. Soc.*, **125,** 3563–3599.

Fofonoff, N. P., 1962: Dynamics of ocean currents. *The Sea.* Vol.1: *Ideas and Observations on Progress in the Study of the Seas, Physical Oceanography*, Vol. 1, M. N. Hill, Ed., John Wiley and Sons, 323–395.

——, and R. M. Hendry, 1985: Current variability near the southeast Newfoundland Ridge. *J. Phys. Oceanogr.*, **15,** 963–984.

Harvey, J., and M. Arhan, 1988: The water masses of the central North Atlantic in 1983–1984. *J. Phys. Oceanogr.*, **18,** 1856–1875.

——, P. Y. Le Traon, and R. Morrow, 1995: Mapping mesoscale variability of the Azores Current using TOPEX/Poseidon and *ERS1* altimetry, together with hydrographic and Lagrangian measurements. *J. Geophys. Res.*, **100** (C12), 24 995–25 006.

Joly, A., and Coauthors, 1999: Overview of the field phase of the Fronts and Atlantic Storm-Track Experiment (FASTEX) project. *Quart. J. Roy. Meteor. Soc.*, **125,** 3131–3163.

Käse, R. H., and W. Krauss, 1996: The Gulf Stream, the North Atlantic Current and the origin of the Azores Current. *The Warmwatersphere of the North Atlantic Ocean.* W. Krauss, Ed., Gebrüder Borntraeger, 291–337.

Kearns, E. J., and H. T. Rossby, 1998: Historical position of the North Atlantic Current. *J. Geophys. Res.*, **103** (C8), 15 509–15 524.

Koblinsky, C. J., P. Gaspar, and G. Lagerloef, 1992: *The Future of Spaceborne Altimetry: Ocean and Climate Change.* Joint Oceanographic Institution, Inc., 75 pp.

Krauss, W., 1986: The North Atlantic Current. *J. Geophys. Res.*, **91,** 5061–5074.

——, and R. H. Käse, 1984: Mean circulation and eddy kinetic energy in the eastern North Atlantic. *J. Geophys. Res.*, **89,** 3407–3415.

——, ——, and H. H. Heinrichsen, 1990: The branching of the Gulf Stream southeast of the Grand Banks. *J. Geophys. Res.*, **95,** 13 089–13 103.

Lazier, J., 1994: Observations in the northwest corner of the North Atlantic Current. *J. Phys. Oceanogr.*, **24,** 1449–1463.

Le Traon, P.-Y., and F. Ogor, 1998: *ERS-1/2* orbit improvement using TOPEX/Poseidon: The 2 cm challenge. *J. Geophys. Res.*, **103,** 8045–8057.

——, and G. Dibarboure, 1999: Mesoscale mapping capabilities of multiple-satellite altimeter missions. *J. Atmos. Oceanic Technol.*, **16,** 1208–1223.

——, M. C. Rouquet, and C. Boissier, 1990: Spatial scales of mesoscale variability in the North Atlantic as deduced from Geosat data. *J. Geophys. Res.*, **95,** 20 267–20 285.

——, F. Nadal, and N. Ducet, 1998: An improved mapping method of multi-satellite altimeter data. *J. Atmos. Oceanic Technol.*, **15,** 522–534.

Lozier, M. S., W. Brechner Owens, and R. G. Curry, 1995: The climatology of the North Atlantic. *Progress in Oceanography*, Vol. 36, Pergamon, 1–44.

Mann, C. R., 1967: The termination of the Gulf Stream and the beginning of the North Atlantic Current. *Deep-Sea Res. Oceanogr. Abstr.*, **14,** 337–359.

McLellan, H. J., 1957: On the distinctness and origin of the slope off the Scotian Shelf and its easterly flow south of the Grand Banks. *J. Fish. Res. Bd. Can.*, **14,** 213–239.

Reynaud, T. H., A. J. Weaver, and Greatbatch, 1995: Summer mean circulation of the Northwestern Atlantic Ocean. *J. Geophys. Res.*, **100,** 779–816.

Richardson, P. L., 1983: Eddy kinetic energy in the North Atlantic from surface drifters. *J. Geophys. Res.*, **88,** 4355–4367.

Rossby, H. T., 1996: The North Atlantic Current and surrounding waters: At the crossroads. *Rev. Geophys.*, **34,** 463–481.

——, 1999: On gyre interactions. *Deep-Sea Res. II*, **46,** 139–164.

Rutherford, I. D., 1972: Data assimilation by statistical interpolation of forecast error fields. *J. Atmos. Sci.*, **29,** 809–815.

Schmitz, W. J., Jr., 1985: SOFAR float trajectories associated with the Newfoundland Basin. *J. Mar. Res.*, **43,** 761–778.

——, and M. S. McCartney, 1993: On the North Atlantic circulation. *Rev. Geophys.*, **31,** 29–49.

Soule, F. M., 1951: Physical oceanography of the Grand Banks region, Labrador Sea and Davis Strait in 1938. *Bull. U.S. Coast Guard*, **28,** 113–173.

Sy, A., 1988: Investigation of large-scale circulation patterns in the central North Atlantic: The North Atlantic Current, the Azores Current, and the Mediterranean Water plume in the area of the Mid-Atlantic Ridge. *Deep-Sea Res.*, **35,** 383–413.

——, U. Schauer, and J. Meincke, 1992: The North Atlantic Current and its associated hydrographic structure above and eastwards of the Mid-Atlantic Ridge. *Deep-Sea Res.*, **39,** 825–853.

Willebrand, J., R. H. Käse, D. Stammer, H. H. Hinrichsen, and W. Krauss, 1990: Verification of Geosat sea surface topography in the Gulf Stream extension with surface drifting buoys and hydrographic measurements. *J. Geophys. Res.*, **95,** 3007–3014.

Worthington, L. V., 1976: On the North Atlantic circulation. *Johns Hopkins Oceanogr. Stud.*, No. 6, 110 pp.